Title

Fibrinogen Activates BMP Signaling in Oligodendrocyte Progenitor Cells and Inhibits Remyelination after Vascular Damage

Journal

Neuron, 96(5)

ISSN

0896-6273

Authors

Petersen, Mark A
Ryu, Jae Kyu
Chang, Kae-Jiun
et al.

Publication Date

2017-12-01

DOI

10.1016/j.neuron.2017.10.008

Peer reviewed

Report

Neuron

Fibrinogen Activates BMP Signaling in Oligodendrocyte Progenitor Cells and Inhibits Remyelination after Vascular Damage

Highlights

- Fibrinogen is a blood-derived inhibitor of oligodendrocyte differentiation
- Fibrinogen induces the BMP receptor pathway in OPCs
- The ACVR1 inhibitor DMH1 blocks fibrinogen's inhibitory effects on OPCs
- Depletion of fibrinogen promotes remyelination in the CNS

Authors

Mark A. Petersen, Jae Kyu Ryu, Kae-Jiun Chang, ..., David H. Rowitch, Jonah R. Chan, Katerina Akassoglou

Correspondence

kakassoglou@gladstone.ucsf.edu

In Brief

Extrinsic inhibitors contribute to remyelination failure in neurological diseases. Petersen et al. identify the blood coagulation factor fibrinogen as an activator of BMP receptor signaling in oligodendrocyte progenitor cells that may be targeted therapeutically to promote remyelination.

Petersen et al., 2017, Neuron *96*, 1–10
December 6, 2017
https://doi.org/10.1016/j.neuron.2017.10.008

CellPress

Please cite this article in press as: Petersen et al., Fibrinogen Activates BMP Signaling in Oligodendrocyte Progenitor Cells and Inhibits Remyelination after Vascular Damage, Neuron (2017), https://doi.org/10.1016/j.neuron.2017.10.008

Neuron
Report

Fibrinogen Activates BMP Signaling in Oligodendrocyte Progenitor Cells and Inhibits Remyelination after Vascular Damage

Mark A. Petersen,[1,2] Jae Kyu Ryu,[1,19] Kae-Jiun Chang,[3,19] Ainhoa Etxeberria,[3] Sophia Bardehle,[1] Andrew S. Mendiola,[1] Wanjiru Kamau-Devers,[1,4] Stephen P.J. Fancy,[2,3,5] Andrea Thor,[6] Eric A. Bushong,[6] Bernat Baeza-Raja,[1] Catriona A. Syme,[1] Michael D. Wu,[1,7] Pamela E. Rios Coronado,[1] Anke Meyer-Franke,[1] Stephanie Yahn,[8] Lauriane Pous,[9] Jae K. Lee,[8] Christian Schachtrup,[10] Hans Lassmann,[11] Eric J. Huang,[12] May H. Han,[13] Martina Absinta,[14] Daniel S. Reich,[14] Mark H. Ellisman,[6,15,16] David H. Rowitch,[2,17,18] Jonah R. Chan,[3] and Katerina Akassoglou[1,3,20,*]
[1]Gladstone Institutes, San Francisco, CA, USA
[2]Department of Pediatrics
[3]Department of Neurology
University of California, San Francisco, CA, USA
[4]Berkeley City College, Berkeley, CA, USA
[5]Newborn Brain Research Institute, University of California, San Francisco, CA, USA
[6]National Center for Microscopy and Imaging Research, Center for Research in Biological Systems, University of California, San Diego, La Jolla, CA, USA
[7]Department of Anesthesia, University of California, San Francisco, CA, USA
[8]Miami Project to Cure Paralysis, Department of Neurological Surgery, University of Miami Miller School of Medicine, Miami, FL, USA
[9]Faculty of Biology
[10]Institute of Anatomy and Cell Biology, Faculty of Medicine
University of Freiburg, Freiburg, Germany
[11]Center for Brain Research, Medical University of Vienna, Vienna, Austria
[12]Department of Pathology, University of California, San Francisco, CA, USA
[13]Department of Neurology and Neurological Sciences, Stanford University School of Medicine, Stanford, CA, USA
[14]Translational Neuroradiology Section, National Institute of Neurological Disorders and Stroke, National Institutes of Health, Bethesda, MD, USA
[15]Department of Neurosciences, University of California, San Diego, La Jolla, California, USA
[16]Salk Institute for Biological Studies, La Jolla, San Diego, California, USA
[17]Department of Neurosurgery, Eli and Edythe Broad Institute for Stem Cell Research and Regeneration Medicine, University of California, San Francisco, CA, USA
[18]Department of Paediatrics, University of Cambridge, Cambridge, UK
[19]These authors contributed equally
[20]Lead Contact
*Correspondence: kakassoglou@gladstone.ucsf.edu
https://doi.org/10.1016/j.neuron.2017.10.008

SUMMARY

Blood-brain barrier (BBB) disruption alters the composition of the brain microenvironment by allowing blood proteins into the CNS. However, whether blood-derived molecules serve as extrinsic inhibitors of remyelination is unknown. Here we show that the coagulation factor fibrinogen activates the bone morphogenetic protein (BMP) signaling pathway in oligodendrocyte progenitor cells (OPCs) and suppresses remyelination. Fibrinogen induces phosphorylation of Smad 1/5/8 and inhibits OPC differentiation into myelinating oligodendrocytes (OLs) while promoting an astrocytic fate *in vitro*. Fibrinogen effects are rescued by BMP type I receptor inhibition using dorsomorphin homolog 1 (DMH1) or CRISPR/Cas9 activin A receptor type I (*ACVR1*) knockout in OPCs. Fibrinogen and the BMP target Id2 are increased in demyelinated multiple sclerosis (MS) lesions. Therapeutic depletion of fibrinogen decreases BMP signaling and enhances remyelination *in vivo*. Targeting fibrinogen may be an upstream therapeutic strategy to promote the regenerative potential of CNS progenitors in diseases with remyelination failure.

INTRODUCTION

Remyelination is critical for recovery in several diseases, such as multiple sclerosis (MS), neonatal white matter injury (NWMI), and stroke (Franklin and Ffrench-Constant, 2008; Rosenzweig and Carmichael, 2015). In these conditions, oligodendrocyte progenitor cells (OPCs) often fail to differentiate into mature oligodendrocytes (OLs) required for myelin repair (Fancy et al., 2011a). However, molecules in the lesion environment that activate pathways in OPCs to inhibit their differentiation are not fully known

(Gallo and Deneen, 2014). OPCs are closely associated with the perivascular niche, which is altered when increased blood-brain barrier (BBB) permeability allows blood proteins into the CNS (Tsai et al., 2016; Zlokovic, 2008). The contribution of blood-derived signals to OPC dysfunction is unknown. Identifying upstream blood-derived signals that dysregulate the progenitor niche may open novel therapeutic strategies for remyelination.

Fibrinogen, a blood coagulation protein, is deposited in many CNS diseases with BBB disruption and myelin abnormalities, including MS, stroke, traumatic brain injury, and Alzheimer's disease (Bardehle et al., 2015; Davalos et al., 2012). Fibrinogen is found in the progressive MS cortex and in active and chronic MS lesions (Vos et al., 2005; Yates et al., 2017). BBB disruption and fibrinogen deposition occur early in MS and precede demyelination (Marik et al., 2007). Progressive MS cases with abundant cortical fibrinogen deposition have perturbed fibrinolysis and reduced neuronal density (Yates et al., 2017). Fibrinogen is not just a marker of BBB disruption, but a driver of neuropathology (Bardehle et al., 2015). It promotes neuroinflammation and glial scar formation by direct effects on microglia, astrocytes, and neurons (Adams et al., 2007; Davalos et al., 2012; Schachtrup et al., 2010). Since fibrinogen regulates functions of CNS cells and is found in MS lesions, we hypothesized that fibrinogen may influence OPCs and remyelination.

RESULTS

Fibrinogen Inhibits OPC Differentiation and Myelination

To test effects of fibrinogen on myelination, we treated primary cultures of rat cortical OPCs with fibrinogen. Fibrinogen inhibited OPC differentiation into mature OLs shown by decreased myelin basic protein (MBP)+ OLs and MBP gene and protein expression (Figures 1A and 1B). Fibrinogen did not affect OPC apoptosis or proliferation (Figures S1A–S1C). In OPC/dorsal root ganglion (DRG) myelinating co-cultures, fibrinogen inhibited axonal myelination, reducing mature, myelinating OLs by 60% (Figure 1C). Although some fibrinogen-treated OPCs differentiated to MBP+ OLs, many did not form myelin sheaths, suggesting impaired axonal wrapping (Figure 1C, arrows). In a neuron-free, nanofiber myelinating culture system (Lee et al., 2012), fibrinogen-coated nanofibers inhibited OPC differentiation and myelination compared to control poly(L-lysine)-coated or albumin-coated nanofibers (Figure 1D; Figures S1D–S1F). In fibrinogen-coated nanofiber cultures, the few OPCs that matured to MBP+ cells had a marked deficit in wrapping nanofibers and formed large membrane sheets rather than myelin-like segments (Figure 1D). Fibrinogen is a potent activator of microglia and macrophages (Adams et al., 2007; Ryu et al., 2015). OPCs treated with conditioned media from fibrin-primed macrophages reduced differentiation to MBP+ cells (Figure S1G), suggesting that fibrinogen exerts immune-mediated and cell-autonomous inhibition of OPC differentiation. In human MS lesions and NWMI, OPCs expressing the high-activity Wnt marker RNF43 (Fancy et al., 2014) were associated with leaky blood vessels and fibrinogen deposits (Figure 1E).

To determine the mechanism mediating fibrinogen's inhibitory effect on OPC differentiation, we used whole-genome microarray of fibrinogen-treated OPCs. Gene ontology (GO) analysis revealed that fibrinogen upregulates the bone morphogenetic protein (BMP) pathway, a major suppressor of OPC differentiation (Gallo and Deneen, 2014) (Figure 1F; Table S1). Fibrinogen increased expression of several BMP-responsive genes (e.g., *Id1*, *Id2*, *Nog*, *Hes1*, *Hey1*, and *Lef1*) (Figure 1F) that are associated with impaired OPC differentiation and upregulated in some MS patients (Pedre et al., 2011; Wu et al., 2012). We evaluated brain autopsy samples of patients with different types of MS lesions by immunostaining for fibrinogen and MBP or the BMP target Id2. We compared active lesions, characterized by florid parenchymal inflammation and ongoing demyelination, chronic lesions of demyelinated areas with absent or few inflammatory cells, and remyelinated lesions (Absinta et al., 2016; Han et al., 2008). Active lesions had high levels of Id2 in areas of fibrinogen deposition and demyelination (Figures 2A–2C). Perivascular fibrinogen was detected in chronic MS lesions but was minimal in remyelinated lesions and absent in normal white matter (Figures 2A and 2B). Id2 expression was reduced in the chronic lesions and similar to controls in remyelinated lesions (Figures 2A and 2B). These results suggest that fibrinogen is associated with increased BMP signaling at sites of increased BBB permeability.

Fibrinogen Activates BMP Receptor Signaling in OPCs

In cultured rat OPCs, fibrinogen increased phosphorylation of the BMP signal transducers Smad1/5 and induced *Id1-3* expression (Figures 2D and 2E), indicating activation of BMP downstream signaling. DMH1, a dorsomorphin analog that inhibits the BMP type I receptor ACVR1 (Alk2) (Hao et al., 2010), blocked fibrinogen-induced phosphorylation of Smad1/5 and suppressed the *Id* genes (Figures 2D and 2E). Fibrinogen increased RNA and protein expression of LEF1 (Figures 2F and 2G), which is regulated by ACVR1 and associated with arrested OPC maturation (Choe et al., 2013; Fancy et al., 2014). DMH1 blocked fibrinogen-induced LEF1 expression and increased MBP expression (Figures 2F and 2G), indicating that fibrinogen activates ACVR1 signal transduction to inhibit myelin production.

A striking effect of BMP signaling in OPCs is differentiation to GFAP+ astrocyte-like cells instead of mature OLs *in vitro* (Mabie et al., 1997). Similarly, fibrinogen increased GFAP+ cells in OPC cultures (Figure 2H). To test whether GFAP+ cells in fibrinogen-treated cultures derived from OPCs, we traced the cell fate of OPCs from *NG2-CreER^{TM}:Rosa-tdTomato* mice, allowing tamoxifen-induced expression of a red fluorescent protein, tdTomato, in nerve/glial antigen-2 (NG2)+ OPCs and their progeny (Figure S2A). Fibrinogen reduced formation of mature MBP+ OLs from genetically labeled NG2+ OPCs and increased the proportion of GFAP+ cells in culture (Figure S2B). Chronic infusion of fibrinogen into brains of *NG2-CreER^{TM}:Rosa-tdTomato* mice increased the percentage of tdTomato+ cells expressing GFAP (Figure S2C), suggesting that fibrinogen induces a similar BMP-like effect *in vivo*.

Fibrinogen Disrupts OPC Differentiation by Activating ACVR1

Noggin, a secreted BMP inhibitor, is a key homeostatic regulator of BMP that binds to extracellular BMPs to antagonize receptor binding (Groppe et al., 2002). Noggin rescued OPCs

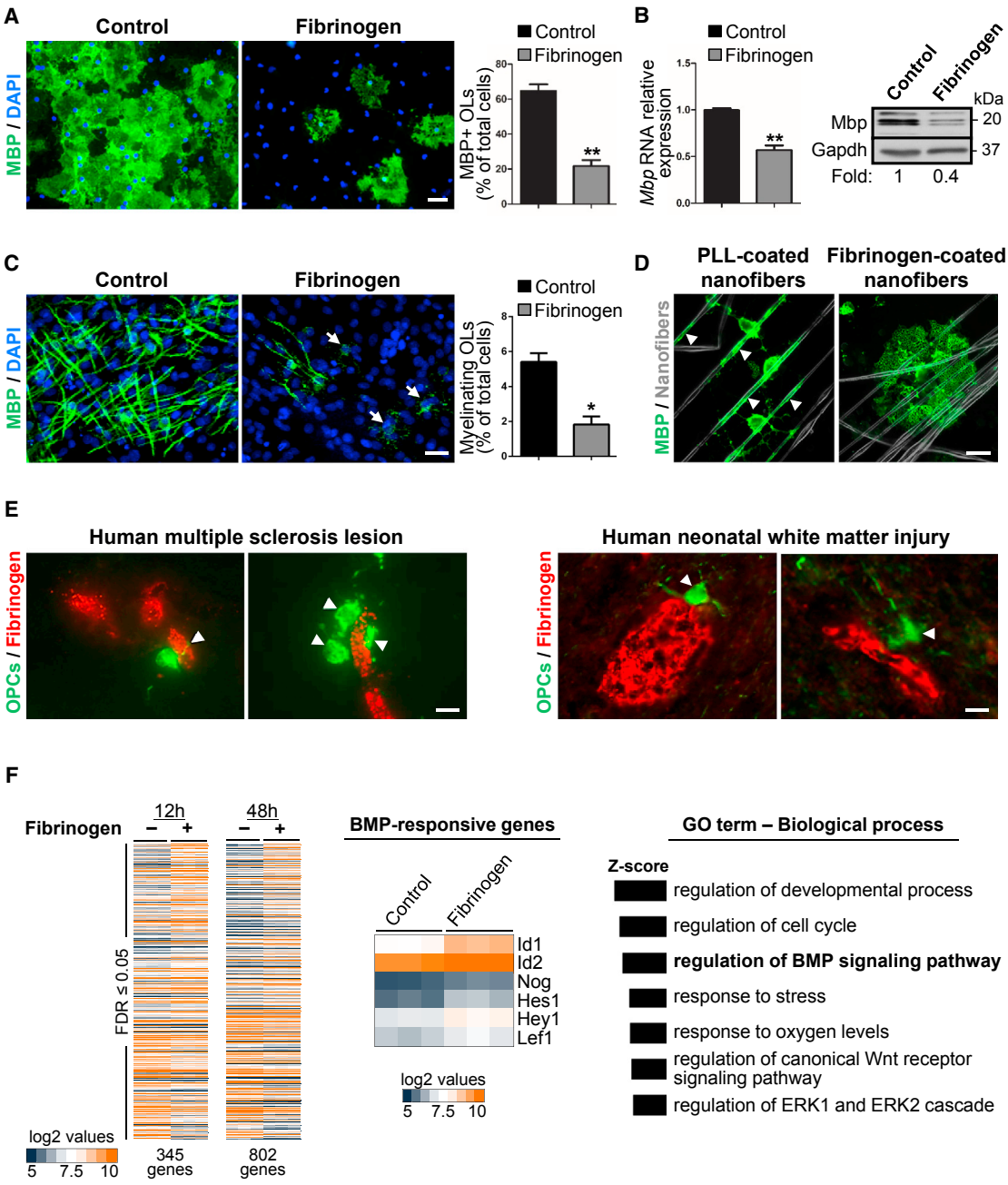

Figure 1. Fibrinogen Inhibits OPC Differentiation and Myelination *In Vitro*

(A) MBP immunostaining (green) indicates mature OLs in control or fibrinogen-treated primary rat OPC cultures after 4 days. Nuclei are stained with DAPI (blue). Representative images from n = 3 independent experiments. Scale bar, 50 μm. Values are mean ± SEM, **p < 0.01 (unpaired t test).

(B) *Mbp* gene (left) and protein (right) expression analysis from control or fibrinogen-treated primary rat OPCs. Values are mean ± SEM from n = 3 independent experiments. **p < 0.01 (unpaired t test). Representative immunoblot from n = 2 independent experiments.

(C) MBP immunostaining (green) indicating mature OLs in OPC-DRG myelinating co-cultures at 7 days *in vitro*. Nuclei are stained with DAPI (blue). Arrows, MBP+ OLs without formed myelin segments. Scale bar, 25 μm. Representative images from n = 3 independent experiments. Values are mean ± SEM, *p < 0.05 (unpaired t test).

(D) MBP+ mature OLs (green) in myelinating cultures of OPCs on control PLL- or fibrinogen-coated nanofibers at 4 days *in vitro*. Representative images from n = 2 independent experiments. Arrowheads, myelin-like segments. Scale bar, 25 μm.

(E) Immunostaining of fibrinogen (red) and RNF43 (green) in the chronic active border of a human MS lesion and the subcortical white matter of an infant with NWMI from hypoxic-ischemic encephalopathy. Arrowheads, RNF43+ cells with bipolar OPC morphology in close proximity to fibrinogen (red). Scale bar, 10 μm.

(F) Whole-genome microarray gene expression analysis of controls and fibrinogen-stimulated rat primary OPCs after 12 and 48 hr of treatment. Heatmap and GO analysis of differentially expressed genes; 345 genes (12 hr) and 802 genes (48 hr) (false discovery rate [FDR] ≤ 0.05). Heatmap of BMP-responsive genes shown at 12 hr of fibrinogen treatment. Log2 values are represented on the heatmaps.

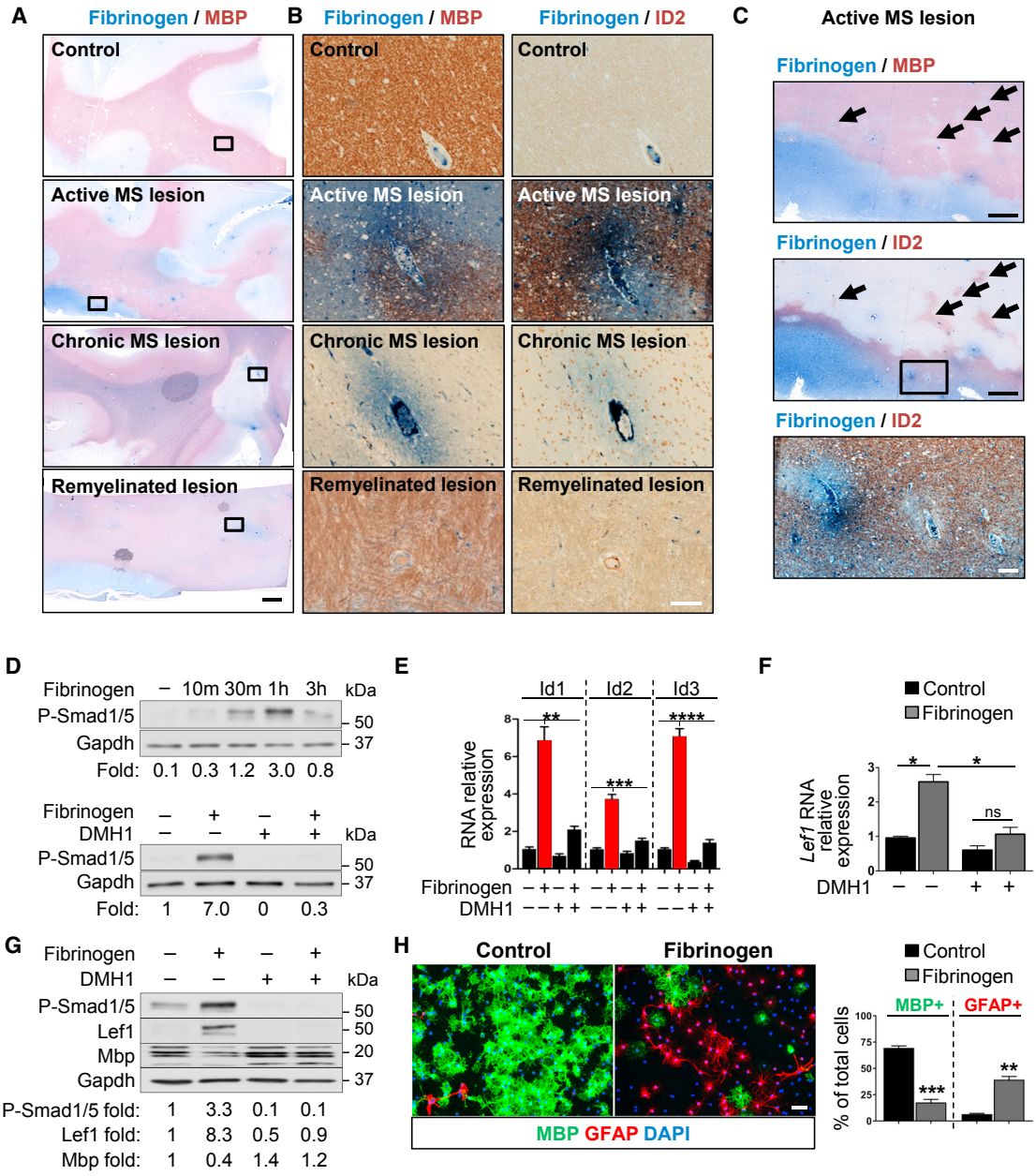

Figure 2. Fibrinogen Activates BMP Signaling in OPCs

(A–C) Immunohistochemistry for fibrinogen (blue) and either MBP (brown) or Id2 (brown) in active, chronic, and remyelinating MS lesions. (A) Boxes show location of images in (B). Scale bar, 2 mm. (B) Scale bar, 100 μm. (C) Box shows location of bottom image. Arrows indicate areas of demyelination with increased Id2 immunoreactivity. Scale bar, 1 mm (top), 100 μm (bottom).

(D) Top: P-Smad1/5 levels in primary rat OPCs treated with fibrinogen for the indicated time. Bottom: P-Smad1/5 levels in control or fibrinogen-treated primary rat OPCs in the presence of the BMP receptor inhibitor DMH1. Values are mean of n = 2 independent experiments.

(E) *Id1-3* in primary rat OPCs treated with fibrinogen for 3 hr and DMH1. Values are mean ± SEM from n = 3 independent experiments. $^{**}p < 0.01$, $^{***}p < 0.001$, $^{****}p < 0.0001$ (two-way ANOVA with Bonferroni).

(F) *Lef1* in primary rat OPCs treated with fibrinogen for 48 hr and DMH1. Values are mean ± SEM from n = 2 independent experiments. ns, not significant, $^{*}p < 0.05$ (two-way ANOVA with Bonferroni).

(G) P-Smad1/5, Lef1, and MBP in primary rat OPCs treated with fibrinogen and DMH1 for 4 days. Representative immunoblot and densitometry from n = 2 independent experiments.

(H) Immunofluorescence for MBP (green) and GFAP (red) in primary rat OPCs treated with fibrinogen or control. Nuclei are stained with DAPI. Representative images from n = 3 independent experiments. Scale bar, 50 μm. Values are mean ± SEM, $^{**}p < 0.01$, $^{***}p < 0.001$ (unpaired t test).

from the inhibitory effects of BMPs *in vitro* but failed to block fibrinogen (Figures 3A and 3B). By ELISA, fibrinogen had no free BMP-2, -4, or -7 (data not shown). Unlike noggin, DMH1 blocks BMP signaling by antagonizing the intracellular kinase domain of ACVR1 (Hao et al., 2010). DMH1 rescued OPCs from the inhibitory effects of BMP-7, an ACVR1 ligand, but not BMP-4, which does not act through ACVR1, showing the selectivity of DMH1 for ACVR1 (Figure 3A). In fibrinogen-treated OPCs, DMH1 increased the number of mature OLs, decreased the GFAP+ cells, and suppressed fibrinogen-induced *Id1* gene expression (Figures 3A and 3B). Knockout of ACVR1 in primary OPCs by CRISPR/Cas9 reduced fibrinogen-induced nuclear accumulation of phosphorylated Smad1/5 and *Id1* expression and enhanced formation of mature MBP+ OLs after fibrinogen treatment (Figure 3C; Figures S3A–S3C). In the HAP1 human cell line, ACVR1 CRISPR/Cas9 knockout suppressed fibrinogen-induced *Id1* (Figure S3D). Lipid rafts regulate BMP receptor signaling and progenitor cell differentiation (North et al., 2015). Pre-treating OPCs with the lipid raft disrupting methyl-β-cyclodextrin reduced fibrinogen-induced phospho-Smad1/5 levels by ~45% (Figure S3E), suggesting that fibrinogen enhances ACVR1 receptor association in lipid rafts to activate BMP signaling. These results suggest fibrinogen overcomes the endogenous homeostatic mechanisms that scavenge free BMPs and inhibits myelination by BMP ligand-independent activation of ACVR1.

Therapeutically Depleting Fibrinogen Increases Remyelination *In Vivo*

To assess OPC differentiation and remyelination *in vivo*, we used the lysolecithin (LPC) focal demyelination model (Fancy et al., 2014). Fibrinogen was deposited in LPC lesions, suggesting BBB disruption (Figure 4A), which was cleared by 10–14 days post-lesion (d.p.l.), when remyelination begins (Figure 4A). To therapeutically deplete fibrinogen in the LPC model, we administered the defibrinogenating agent ancrod at 3 d.p.l. (Adams et al., 2007). Fibrinogen depletion reduced phospho-Smad1/5/8 in demyelinated lesions (Figure 4B), suggesting reduction of BMP receptor pathway activation. Fibrinogen-depleted mice had more mature *PLP*-expressing OLs within LPC lesions (Figure 4C) and enhanced remyelination (Figure 4D), as indicated by a reduced proportion of axons that remained demyelinated and a decreased G ratio of remyelinated axons, which indicates thicker myelin. Ancrod alone did not affect OPC differentiation *in vitro* (Figure S3F), suggesting that the pro-myelinating effect of ancrod is due to fibrinogen depletion.

DISCUSSION

We found that fibrinogen is a potent extrinsic inhibitor of OPC differentiation and remyelination. Fibrinogen activates the ACVR1 receptor on OPCs to induce downstream signaling and BMP target gene expression and inhibit remyelination (Figure 4E). Fibrinogen may be beneficial in acute CNS injuries by acting as a "damage signal" that delays regeneration until the extracellular environment is conducive to repair. But, in chronic diseases with excessive fibrinogen deposition or inadequate fibrinogen clearance, this mechanism may be deleterious and lead to a state akin to a non-healing wound with aberrant activation of signaling pathways that block regeneration. Indeed, persistent fibrin deposition inhibits wound repair and is a feature of chronic MS lesions with impaired fibrinolysis (Bugge et al., 1996; Gveric et al., 2003; Yates et al., 2017). Endogenous homeostatic mechanisms that scavenge free BMPs do not block fibrinogen's inhibitory effects. Thus, targeting fibrinogen therapeutically may tip the balance from a dysregulated environment to one that promotes repair.

Fibrinogen may contribute to a hostile environment in demyelinating diseases by activating BMP receptor signaling in OPCs (this study) and as an upstream driver of inflammation and reactive gliosis (Bardehle et al., 2015). At sites of BBB disruption, fibrinogen is converted to proinflammatory fibrin, which induces reactive oxygen species (ROS) release and M1-like activation of microglia and macrophages (Davalos et al., 2012; Ryu et al., 2015). M1-like polarization of innate immune cells and ROS are toxic to OPCs and hinder remyelination (Back et al., 1998; Lehnardt et al., 2002). A switch from an M1- to an M2-dominant response is essential for remyelination (Miron et al., 2013). Conditioned media from fibrin-treated macrophages hindered OPC differentiation. Fibrin-induced M1-like polarization of microglia and macrophages (Davalos et al., 2012; Ryu et al., 2015) may hinder the reparative inflammatory response for remyelination, which would agree with failed repair of MS lesions, where BBB leakage at the lesion edge is prolonged (Absinta et al., 2016). Fibrinogen depletion with ancrod decreases inflammation and demyelination in animal MS models (Adams et al., 2007; Akassoglou et al., 2004; Paterson, 1976; Ryu et al., 2015). In the LPC model, active demyelination occurs at 1–3 d.p.l. and initial recruitment and activation of inflammatory cells at 12 hr–3 d.p.l. (Mei et al., 2014; Ousman and David, 2000). In our study, ancrod was administered therapeutically starting at 3 d.p.l. to avoid interference with the initial demyelination and inflammation. Ancrod decreased BMP pathway activation and increased synthesis of myelin genes, but we cannot exclude ancrod effects in fibrin-driven inflammation and demyelination after 3 d.p.l. Future studies will determine the relative contributions of fibrinogen actions on OPCs and inflammatory cells in inhibiting remyelination.

Given their pleiotropic functions, fibrinogen and fibrin may affect multiple pathological mechanisms that alter repair. Fibrinogen inhibits Schwann cell differentiation and inhibits neurite outgrowth (Akassoglou et al., 2002; Schachtrup et al., 2007). Fibrinogen induces production of other extrinsic remyelination inhibitors like chondroitin sulfate proteoglycans (CSPGs) in astrocytes and endothelin-1 in endothelial cells (Schachtrup et al., 2010; Sen et al., 2009). Responses to fibrinogen-induced signaling and inflammation in the OL lineage may be dependent on the stage of cell differentiation with differential effects on OPCs, premyelinating OLs, and mature OLs. Thus, fibrinogen may be an apical signal that orchestrates the molecular composition of the inhibitory extracellular environment. An effect of fibrinogen in OPCs consistent with activation of BMP signaling was formation of GFAP+, astrocyte-like cells. OPC multipotency *in vivo* and potential lineage switches in disease are controversial (Richardson et al., 2011). In acute animal models of

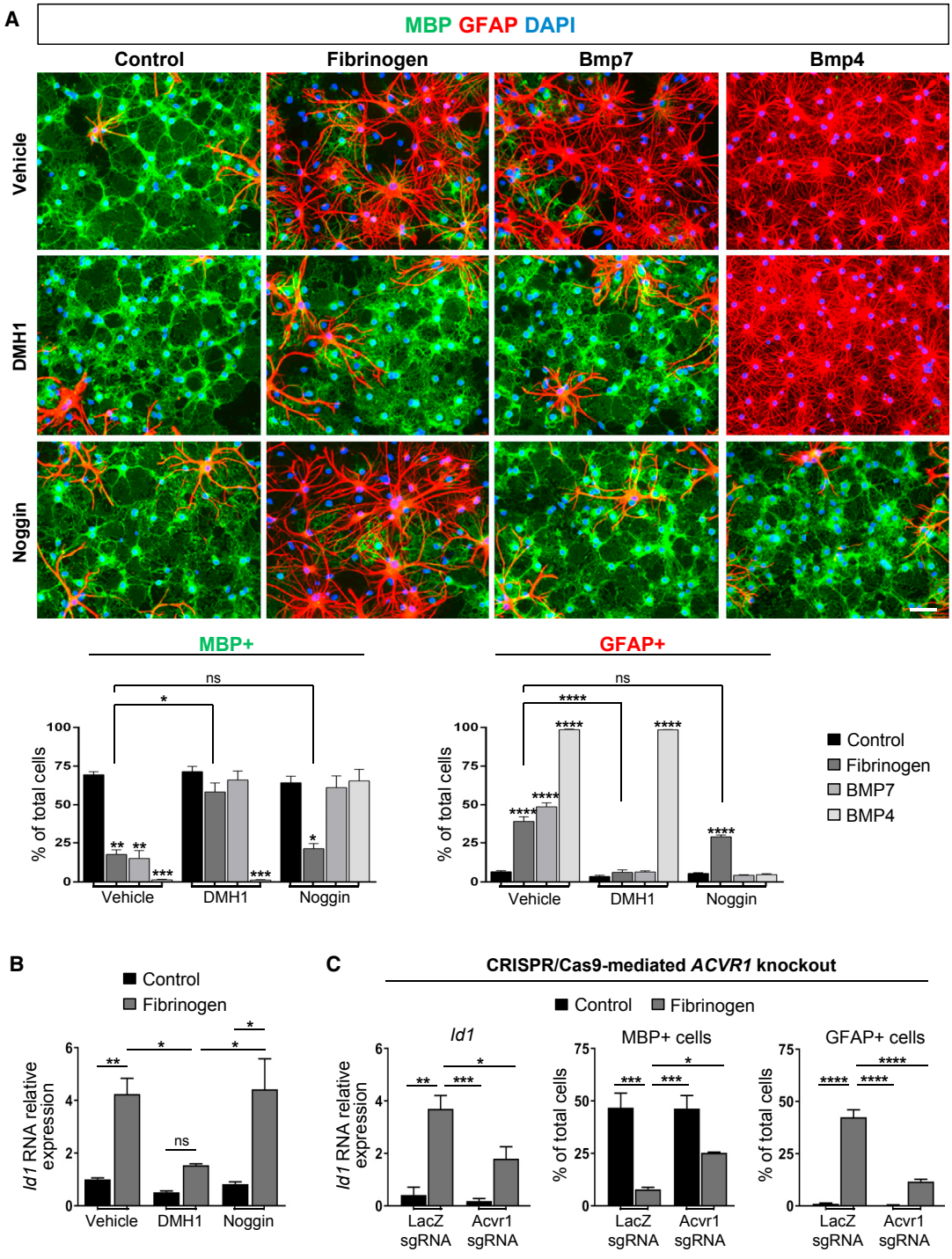

Figure 3. Fibrinogen Disrupts OPC Differentiation through BMP Ligand-Independent Activation of ACVR1

(A) Immunofluorescence for MBP (green) and GFAP (red) in primary rat OPCs treated with fibrinogen, BMP7, or BMP4 and DMH1, noggin, or vehicle control. Nuclei are stained with DAPI. Data are mean ± SEM from n = 2–3 independent experiments. ns, not significant, *p < 0.05, **p < 0.01, ***p < 0.001, ****p < 0.0001 (two-way ANOVA with Bonferroni). Scale bar, 50 μm.

(B) *Id1* in primary rat OPCs treated with fibrinogen and DMH1, noggin, or vehicle control. Values are mean ± SEM from n = 4–7 wells from 2–3 independent experiments. ns, not significant, *p < 0.05, **p < 0.01 (two-way ANOVA with Bonferroni).

(C) Analysis of primary rat OPCs transfected with a Cas9 expression plasmid containing single-guide RNA (sgRNA) for either LacZ (control) or Acvr1. Left: *Id1* after 2 hr fibrinogen treatment, n = 3 independent experiments. Right: quantification of MBP+ and GFAP+ cells after 3 day fibrinogen treatment, n = 4 wells from 2 independent experiments. Values are mean ± SEM, *p < 0.05, **p < 0.01, ***p < 0.001, ****p < 0.0001 (two-way ANOVA with Holm-Sidak).

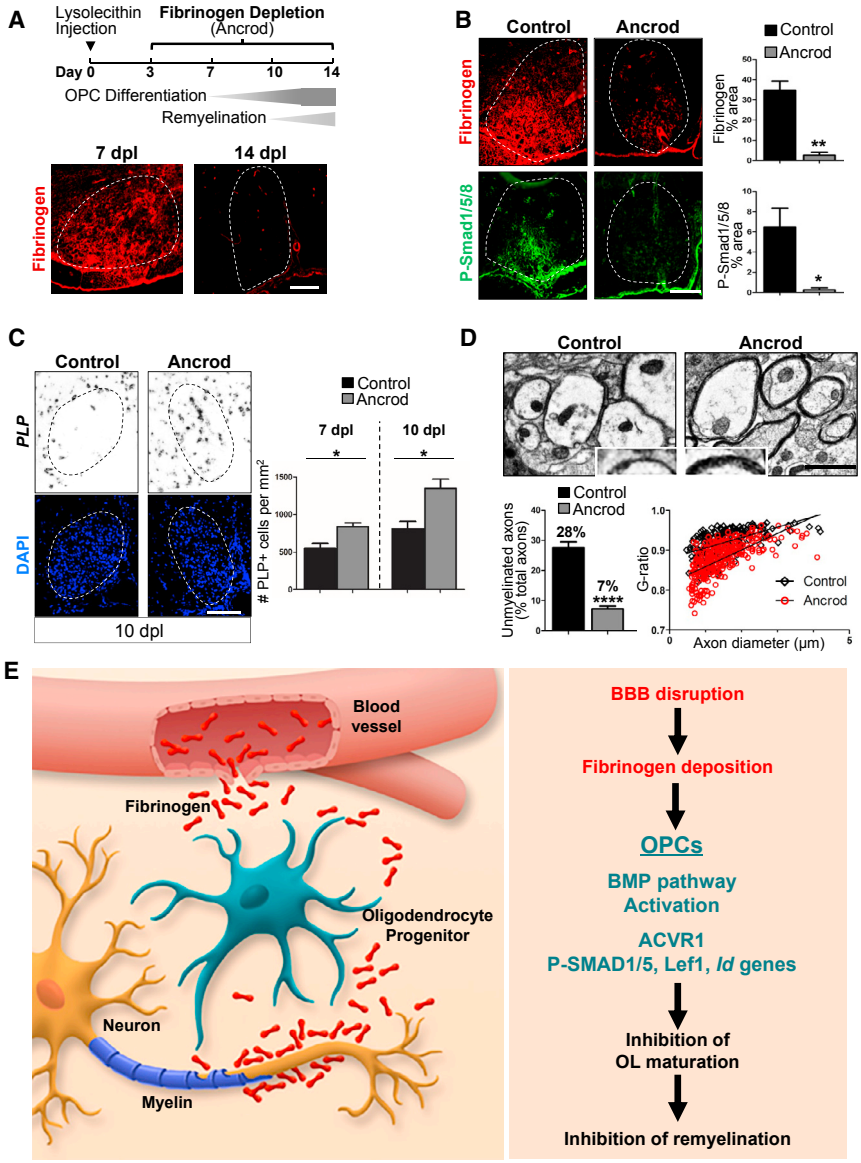

Figure 4. Therapeutically Depleting Fibrinogen Increases Remyelination *In Vivo*

(A) Top: LPC injections with fibrinogen depletion using Ancrod. Bottom: immunostaining for fibrinogen (red) in LPC-induced demyelinated lesions in ventral spinal cord of mice at 7 and 14 d.p.l. Dotted lines, lesion border. Representative images are shown. Scale bar, 100 μm.

(B) Immunostaining for fibrinogen (red) and P-Smad1/5/8 (green) in LPC lesions in ventral spinal cord of mice treated with ancrod or vehicle control at 7 d.p.l. Dotted lines, lesion border. Quantification of fibrinogen and P-Smad1/5/8 immunoreactivity from n = 3 mice per group. Values are mean ± SEM, *p < 0.05, **p < 0.01 (unpaired t test). Scale bar, 100 μm.

(C) *In situ* hybridization for *PLP* mRNA (black) labeling mature OLs in LPC lesions in ventral spinal cord of mice treated with ancrod or vehicle control at 10 d.p.l. Nuclei are stained with DAPI (blue). Dotted lines, lesion border. Quantification of *PLP*+ cells within LPC lesions at 7 and 10 d.p.l. from n = 3–4 mice per group. Values are mean ± SEM, *p < 0.05 (unpaired t test). Scale bar, 100 μm.

(D) Electron microscopy of remyelinating axons within LPC lesions at 14 d.p.l. in ancrod-treated and control mice. Inset image (white box) shows close-up of myelin sheath (black). Quantification of axons within LPC lesions that remained unmyelinated at 14 d.p.l. from n = 4 mice per group. Values are mean ± SEM, ****p < 0.0001 (unpaired t test). G ratios between controls (G ratio mean = 0.92, SEM = 0.002) and the ancrod group (G ratio mean = 0.88, SEM = 0.003). n = ~75 axons counted per mouse, 4 mice per group. ****p < 0.0001 (unpaired t test). Scale bar, 1 μm.

(E) Working model of fibrinogen in CNS remyelination. Fibrinogen enters the CNS after BBB disruption and has pleiotropic functions as an inducer of inflammatory responses and inhibitor of regeneration.

demyelination, such as LPC, the switch of OPCs to astrocytes is a rare event (~3%) (Zawadzka et al., 2010); thus, fibrinogen's inhibitory effect on remyelination in the LPC model is more likely related to inhibiting final OL maturation. Since the LPC model has no permanent remyelination blockade, fibrinogen depletion likely accelerates remyelination. It is possible that fibrinogen-induced BMP signaling drives cell-fate decisions in other models with large or more hemorrhagic insults. Indeed, fate-mapping studies after spinal cord injury show that ~25% of NG2 cells express astrocyte markers (Hackett et al., 2016). Thus, in large traumatic injuries, OPC differentiation to GFAP$^+$ cells may be more pronounced than in acute LPC injection. Fibrinogen is abundantly deposited in the spinal cord after injury (Schachtrup et al., 2007), and chronic fibrinogen infusion is sufficient to increase the number of NG2-derived GFAP$^+$ cells *in vivo* (this study). Future studies will determine whether fibrinogen is required for the generation of astrocyte-like cells by OPCs and stem/progenitor cell-fate determination at sites of vascular damage in animal models with chronic insults. In addition, characterizing the expression of BMP activation markers in OPCs and astrocytes in acute and chronic MS lesions would shed light on this process in human disease.

Our study suggests that targeting fibrinogen may overcome the inhibitory environment that persists in chronically demyelinated lesions. Although screens of FDA-approved drugs identified those that promote myelination (Mei et al., 2014; Najm et al., 2015), it is unknown whether these drugs will overcome inhibition by extrinsic factors in the demyelinated lesions. OPC differentiation drugs failed to rescue inhibition of OPC differentiation by extracellular CSPGs (Keough et al., 2016), suggesting a need for new approaches to target extrinsic inhibition of remyelination. With the many functions of fibrinogen as an OPC

differentiation inhibitor with pro-inflammatory and pro-fibrotic functions, anti-coagulant therapies that inhibit fibrin formation or inhibition of fibrinogen binding to immune cell receptors or growth factors might be beneficial for tissue repair. Counteracting inhibitory BMP signaling in OPCs by BMP receptor inhibitors like DMH1 (our study) or pro-myelinating ligands like activin B (Dutta et al., 2014) may alleviate the inhibitory effects of fibrinogen on remyelination. Novel inhibitors may overcome the hostile, dysregulated environment that persists in chronically demyelinated lesions and open new therapeutic strategies to promote regeneration in neurological diseases with fibrin deposition.

STAR★METHODS

Detailed methods are provided in the online version of this paper and include the following:

- KEY RESOURCES TABLE
- CONTACT FOR REAGENT AND RESOURCE SHARING
- EXPERIMENTAL MODEL AND SUBJECT DETAILS
  - Animals
  - Primary OPC Cultures
  - OPC-DRG Cultures
  - OPC-Nanofiber Cultures
  - Macrophage Conditioned Media
  - HAP1 Cell Cultures
  - Human MS and Neonatal HIE Tissue
- METHOD DETAILS
  - Fibrinogen and Pharmacologic Inhibitors
  - Myelinating Cultures
  - Cell Fate Mapping Studies
  - CRISPR/Cas9-Mediated Knockout of Acvr1 in Primary OPCs
  - RNA Isolation and Quantitative PCR
  - Gene-Expression Profiling by Microarray Analysis
  - Immunoblots
  - Immunocytochemistry, Immunohistochemistry, and *In Situ* Hybridization
  - Chronic Fibrinogen Infusion
  - Lysolecithin-Induced Focal Demyelination
  - Pharmacologic Depletion of Fibrinogen after Lysolecithin Injection
  - Electron Microscope Analysis of Remyelination
- QUANTIFICATION AND STATISTICAL ANALYSIS
- DATA AND SOFTWARE AVAILABILITY

SUPPLEMENTAL INFORMATION

Supplemental Information includes three figures and two tables and can be found with this article online at https://doi.org/10.1016/j.neuron.2017.10.008.

AUTHOR CONTRIBUTIONS

M.A.P. designed, performed experiments, and analyzed data; J.K.R. performed *in vivo* studies; K.-J.C. performed CRISPR studies; A.E. performed *in vitro* studies; S.B. performed cell sorting, histology, and quantification. A.S.M. performed *in vitro* studies and quantification. W.K.-D. performed *in vitro* studies and animal care; S.P.J.F. performed histology; A.T. and E.A.B. performed electron microscopy; B.B.-R. performed immunoblots; C.A.S., M.D.W., and P.E.R.C. performed image analysis and quantification; A.M.-F. performed *in vitro* experiments and ELISAs; E.J.H. procured human neonatal brain tissue; M.H.H., M.A., and D.S.R. provided human MS tissue and analyzed and interpreted data. S.Y., J.K.L., L.P., C.S., and H.L. analyzed and interpreted data. M.H.E., D.H.R., and J.R.C. designed experiments and interpreted data; K.A. and M.A.P. conceived and designed the study, analyzed and interpreted data, and wrote the manuscript with input from all authors.

ACKNOWLEDGMENTS

We thank Reshmi Tognatta for discussions; Belinda Cabriga, Yun-An Shen, Marielle Cavrois, and Nandhini Raman for expert technical assistance; John Lewis for graphics; and Gary Howard for editorial. The Gladstone FACS core was supported by NIH P30 AI027763, NIH S10 RR028962, Department of Defense (DoD) W81XWH-11-1-0562, and the Gladstone Institutes from a National Center for Research Resources Grant RR18928. This work was supported by NIH/NICHD K12-HD072222 grant and Pediatric Scientist Development Program fellowship (March of Dimes 4-FY10-461 and NIH/NICHD K12-HD000850) to M.A.P.; A Race to Erase MS Young Investigator Award and American Heart Association Scientist Development Grant 16SDG30170014 to J.K.R.; National Multiple Sclerosis Society (NMSS) fellowship grants FG-2093-A-1 to M.A. and FG-1507-05195 to K.J.C.; the Marilyn Hilton Bridging Award for Physician-Scientists to M.A., the NINDS Intramural Research Program to D.S.R.; NIH R01 NS027177, R01 GM086197, and P41 GM103412 to M.H.E. for support of the National Center for Microscopy and Imaging Research; the NMSS RG5203, NIH/NINDS R01 NS062796, and the Rachleff Endowment to J.R.C.; and the NIH/NINDS R35 NS097976, NMSS RG4985, DoD MS160082, and Conrad N. Hilton Foundation grants to K.A. K.A. is a co-founder of MedaRed, Inc., and K.A., J.K.R., and A.M.F. are named inventors on patents and patent applications related to fibrin. Their interests are managed by the Gladstone Institutes in accordance with its conflict of interest policy.

Received: October 21, 2016
Revised: August 30, 2017
Accepted: October 4, 2017
Published: November 2, 2017

REFERENCES

Absinta, M., Sati, P., Schindler, M., Leibovitch, E.C., Ohayon, J., Wu, T., Meani, A., Filippi, M., Jacobson, S., Cortese, I.C., and Reich, D.S. (2016). Persistent 7-tesla phase rim predicts poor outcome in new multiple sclerosis patient lesions. J. Clin. Invest. *126*, 2597–2609.

Adams, R.A., Bauer, J., Flick, M.J., Sikorski, S.L., Nuriel, T., Lassmann, H., Degen, J.L., and Akassoglou, K. (2007). The fibrin-derived gamma377-395 peptide inhibits microglia activation and suppresses relapsing paralysis in central nervous system autoimmune disease. J. Exp. Med. *204*, 571–582.

Akassoglou, K., Yu, W.M., Akpinar, P., and Strickland, S. (2002). Fibrin inhibits peripheral nerve remyelination by regulating Schwann cell differentiation. Neuron *33*, 861–875.

Akassoglou, K., Adams, R.A., Bauer, J., Mercado, P., Tseveleki, V., Lassmann, H., Probert, L., and Strickland, S. (2004). Fibrin depletion decreases inflammation and delays the onset of demyelination in a tumor necrosis factor transgenic mouse model for multiple sclerosis. Proc. Natl. Acad. Sci. USA *101*, 6698–6703.

Back, S.A., Gan, X., Li, Y., Rosenberg, P.A., and Volpe, J.J. (1998). Maturation-dependent vulnerability of oligodendrocytes to oxidative stress-induced death caused by glutathione depletion. J. Neurosci. *18*, 6241–6253.

Bardehle, S., Rafalski, V.A., and Akassoglou, K. (2015). Breaking boundaries-coagulation and fibrinolysis at the neurovascular interface. Front. Cell. Neurosci. *9*, 354.

Bugge, T.H., Kombrinck, K.W., Flick, M.J., Daugherty, C.C., Danton, M.J., and Degen, J.L. (1996). Loss of fibrinogen rescues mice from the pleiotropic effects of plasminogen deficiency. Cell *87*, 709–719.

Choe, Y., Kozlova, A., Graf, D., and Pleasure, S.J. (2013). Bone morphogenic protein signaling is a major determinant of dentate development. J. Neurosci. *33*, 6766–6775.

Davalos, D., and Akassoglou, K. (2012). Fibrinogen as a key regulator of inflammation in disease. Semin. Immunopathol. *34*, 43–62.

Davalos, D., Ryu, J.K., Merlini, M., Baeten, K.M., Le Moan, N., Petersen, M.A., Deerinck, T.J., Smirnoff, D.S., Bedard, C., Hakozaki, H., et al. (2012). Fibrinogen-induced perivascular microglial clustering is required for the development of axonal damage in neuroinflammation. Nat. Commun. *3*, 1227.

Dugas, J.C., and Emery, B. (2013). Purification of oligodendrocyte precursor cells from rat cortices by immunopanning. Cold Spring Harb. Protoc. *2013*, 745–758.

Dutta, D.J., Zameer, A., Mariani, J.N., Zhang, J., Asp, L., Huynh, J., Mahase, S., Laitman, B.M., Argaw, A.T., Mitiku, N., et al. (2014). Combinatorial actions of Tgfβ and Activin ligands promote oligodendrocyte development and CNS myelination. Development *141*, 2414–2428.

Emery, B., and Dugas, J.C. (2013). Purification of oligodendrocyte lineage cells from mouse cortices by immunopanning. Cold Spring Harb. Protoc. *2013*, 854–868.

Fancy, S.P., Chan, J.R., Baranzini, S.E., Franklin, R.J., and Rowitch, D.H. (2011a). Myelin regeneration: a recapitulation of development? Annu. Rev. Neurosci. *34*, 21–43.

Fancy, S.P., Harrington, E.P., Yuen, T.J., Silbereis, J.C., Zhao, C., Baranzini, S.E., Bruce, C.C., Otero, J.J., Huang, E.J., Nusse, R., et al. (2011b). Axin2 as regulatory and therapeutic target in newborn brain injury and remyelination. Nat. Neurosci. *14*, 1009–1016.

Fancy, S.P., Harrington, E.P., Baranzini, S.E., Silbereis, J.C., Shiow, L.R., Yuen, T.J., Huang, E.J., Lomvardas, S., and Rowitch, D.H. (2014). Parallel states of pathological Wnt signaling in neonatal brain injury and colon cancer. Nat. Neurosci. *17*, 506–512.

Franklin, R.J., and Ffrench-Constant, C. (2008). Remyelination in the CNS: from biology to therapy. Nat. Rev. Neurosci. *9*, 839–855.

Gallo, V., and Deneen, B. (2014). Glial development: the crossroads of regeneration and repair in the CNS. Neuron *83*, 283–308.

Groppe, J., Greenwald, J., Wiater, E., Rodriguez-Leon, J., Economides, A.N., Kwiatkowski, W., Affolter, M., Vale, W.W., Izpisua Belmonte, J.C., and Choe, S. (2002). Structural basis of BMP signalling inhibition by the cystine knot protein Noggin. Nature *420*, 636–642.

Gveric, D., Herrera, B., Petzold, A., Lawrence, D.A., and Cuzner, M.L. (2003). Impaired fibrinolysis in multiple sclerosis: a role for tissue plasminogen activator inhibitors. Brain *126*, 1590–1598.

Hackett, A.R., Lee, D.H., Dawood, A., Rodriguez, M., Funk, L., Tsoulfas, P., and Lee, J.K. (2016). STAT3 and SOCS3 regulate NG2 cell proliferation and differentiation after contusive spinal cord injury. Neurobiol. Dis. *89*, 10–22.

Han, M.H., Hwang, S.I., Roy, D.B., Lundgren, D.H., Price, J.V., Ousman, S.S., Fernald, G.H., Gerlitz, B., Robinson, W.H., Baranzini, S.E., et al. (2008). Proteomic analysis of active multiple sclerosis lesions reveals therapeutic targets. Nature *451*, 1076–1081.

Hao, J., Ho, J.N., Lewis, J.A., Karim, K.A., Daniels, R.N., Gentry, P.R., Hopkins, C.R., Lindsley, C.W., and Hong, C.C. (2010). In vivo structure-activity relationship study of dorsomorphin analogues identifies selective VEGF and BMP inhibitors. ACS Chem. Biol. *5*, 245–253.

Keough, M.B., Rogers, J.A., Zhang, P., Jensen, S.K., Stephenson, E.L., Chen, T., Hurlbert, M.G., Lau, L.W., Rawji, K.S., Plemel, J.R., et al. (2016). An inhibitor of chondroitin sulfate proteoglycan synthesis promotes central nervous system remyelination. Nat. Commun. *7*, 11312.

Lee, S., Leach, M.K., Redmond, S.A., Chong, S.Y., Mellon, S.H., Tuck, S.J., Feng, Z.Q., Corey, J.M., and Chan, J.R. (2012). A culture system to study oligodendrocyte myelination processes using engineered nanofibers. Nat. Methods *9*, 917–922.

Lehnardt, S., Lachance, C., Patrizi, S., Lefebvre, S., Follett, P.L., Jensen, F.E., Rosenberg, P.A., Volpe, J.J., and Vartanian, T. (2002). The toll-like receptor TLR4 is necessary for lipopolysaccharide-induced oligodendrocyte injury in the CNS. J. Neurosci. *22*, 2478–2486.

Mabie, P.C., Mehler, M.F., Marmur, R., Papavasiliou, A., Song, Q., and Kessler, J.A. (1997). Bone morphogenetic proteins induce astroglial differentiation of oligodendroglial-astroglial progenitor cells. J. Neurosci. *17*, 4112–4120.

Madisen, L., Zwingman, T.A., Sunkin, S.M., Oh, S.W., Zariwala, H.A., Gu, H., Ng, L.L., Palmiter, R.D., Hawrylycz, M.J., Jones, A.R., et al. (2010). A robust and high-throughput Cre reporting and characterization system for the whole mouse brain. Nat. Neurosci. *13*, 133–140.

Marik, C., Felts, P.A., Bauer, J., Lassmann, H., and Smith, K.J. (2007). Lesion genesis in a subset of patients with multiple sclerosis: a role for innate immunity? Brain *130*, 2800–2815.

Mei, F., Fancy, S.P.J., Shen, Y.A., Niu, J., Zhao, C., Presley, B., Miao, E., Lee, S., Mayoral, S.R., Redmond, S.A., et al. (2014). Micropillar arrays as a high-throughput screening platform for therapeutics in multiple sclerosis. Nat. Med. *20*, 954–960.

Miron, V.E., Boyd, A., Zhao, J.W., Yuen, T.J., Ruckh, J.M., Shadrach, J.L., van Wijngaarden, P., Wagers, A.J., Williams, A., Franklin, R.J.M., and Ffrench-Constant, C. (2013). M2 microglia and macrophages drive oligodendrocyte differentiation during CNS remyelination. Nat. Neurosci. *16*, 1211–1218.

Najm, F.J., Madhavan, M., Zaremba, A., Shick, E., Karl, R.T., Factor, D.C., Miller, T.E., Nevin, Z.S., Kantor, C., Sargent, A., et al. (2015). Drug-based modulation of endogenous stem cells promotes functional remyelination in vivo. Nature *522*, 216–220.

North, H.A., Pan, L., McGuire, T.L., Brooker, S., and Kessler, J.A. (2015). β1-Integrin alters ependymal stem cell BMP receptor localization and attenuates astrogliosis after spinal cord injury. J. Neurosci. *35*, 3725–3733.

Ousman, S.S., and David, S. (2000). Lysophosphatidylcholine induces rapid recruitment and activation of macrophages in the adult mouse spinal cord. Glia *30*, 92–104.

Paterson, P.Y. (1976). Experimental allergic encephalomyelitis: role of fibrin deposition in immunopathogenesis of inflammation in rats. Fed. Proc. *35*, 2428–2434.

Patrikios, P., Stadelmann, C., Kutzelnigg, A., Rauschka, H., Schmidbauer, M., Laursen, H., Sorensen, P.S., Brück, W., Lucchinetti, C., and Lassmann, H. (2006). Remyelination is extensive in a subset of multiple sclerosis patients. Brain *129*, 3165–3172.

Pedre, X., Mastronardi, F., Bruck, W., López-Rodas, G., Kuhlmann, T., and Casaccia, P. (2011). Changed histone acetylation patterns in normal-appearing white matter and early multiple sclerosis lesions. J. Neurosci. *31*, 3435–3445.

Platt, R.J., Chen, S., Zhou, Y., Yim, M.J., Swiech, L., Kempton, H.R., Dahlman, J.E., Parnas, O., Eisenhaure, T.M., Jovanovic, M., et al. (2014). CRISPR-Cas9 knockin mice for genome editing and cancer modeling. Cell *159*, 440–455.

Richardson, W.D., Young, K.M., Tripathi, R.B., and McKenzie, I. (2011). NG2-glia as multipotent neural stem cells: fact or fantasy? Neuron *70*, 661–673.

Rosenzweig, S., and Carmichael, S.T. (2015). The axon-glia unit in white matter stroke: mechanisms of damage and recovery. Brain Res. *1623*, 123–134.

Ryu, J.K., Petersen, M.A., Murray, S.G., Baeten, K.M., Meyer-Franke, A., Chan, J.P., Vagena, E., Bedard, C., Machado, M.R., Rios Coronado, P.E., et al. (2015). Blood coagulation protein fibrinogen promotes autoimmunity and demyelination via chemokine release and antigen presentation. Nat. Commun. *6*, 8164.

Schachtrup, C., Lu, P., Jones, L.L., Lee, J.K., Lu, J., Sachs, B.D., Zheng, B., and Akassoglou, K. (2007). Fibrinogen inhibits neurite outgrowth via beta 3 integrin-mediated phosphorylation of the EGF receptor. Proc. Natl. Acad. Sci. USA *104*, 11814–11819.

Schachtrup, C., Ryu, J.K., Helmrick, M.J., Vagena, E., Galanakis, D.K., Degen, J.L., Margolis, R.U., and Akassoglou, K. (2010). Fibrinogen triggers astrocyte scar formation by promoting the availability of active TGF-beta after vascular damage. J. Neurosci. *30*, 5843–5854.

Sen, U., Tyagi, N., Patibandla, P.K., Dean, W.L., Tyagi, S.C., Roberts, A.M., and Lominadze, D. (2009). Fibrinogen-induced endothelin-1 production from endothelial cells. Am. J. Physiol. Cell Physiol. *296*, C840–C847.

Slaymaker, I.M., Gao, L., Zetsche, B., Scott, D.A., Yan, W.X., and Zhang, F. (2016). Rationally engineered Cas9 nucleases with improved specificity. Science *351*, 84–88.

Tsai, H.H., Niu, J., Munji, R., Davalos, D., Chang, J., Zhang, H., Tien, A.C., Kuo, C.J., Chan, J.R., Daneman, R., and Fancy, S.P. (2016). Oligodendrocyte precursors migrate along vasculature in the developing nervous system. Science *351*, 379–384.

Vos, C.M., Geurts, J.J., Montagne, L., van Haastert, E.S., Bö, L., van der Valk, P., Barkhof, F., and de Vries, H.E. (2005). Blood-brain barrier alterations in both focal and diffuse abnormalities on postmortem MRI in multiple sclerosis. Neurobiol. Dis. *20*, 953–960.

Wu, M., Hernandez, M., Shen, S., Sabo, J.K., Kelkar, D., Wang, J., O'Leary, R., Phillips, G.R., Cate, H.S., and Casaccia, P. (2012). Differential modulation of the oligodendrocyte transcriptome by sonic hedgehog and bone morphogenetic protein 4 via opposing effects on histone acetylation. J. Neurosci. *32*, 6651–6664.

Yates, R.L., Esiri, M.M., Palace, J., Jacobs, B., Perera, R., and DeLuca, G.C. (2017). Fibrin(ogen) and neurodegeneration in the progressive multiple sclerosis cortex. Ann. Neurol. *82*, 259–270.

Zawadzka, M., Rivers, L.E., Fancy, S.P., Zhao, C., Tripathi, R., Jamen, F., Young, K., Goncharevich, A., Pohl, H., Rizzi, M., et al. (2010). CNS-resident glial progenitor/stem cells produce Schwann cells as well as oligodendrocytes during repair of CNS demyelination. Cell Stem Cell *6*, 578–590.

Zhu, X., Hill, R.A., Dietrich, D., Komitova, M., Suzuki, R., and Nishiyama, A. (2011). Age-dependent fate and lineage restriction of single NG2 cells. Development *138*, 745–753.

Zlokovic, B.V. (2008). The blood-brain barrier in health and chronic neurodegenerative disorders. Neuron *57*, 178–201.

STAR★METHODS

KEY RESOURCES TABLE

REAGENT or RESOURCE	SOURCE	IDENTIFIER
Antibodies		
Rabbit polyclonal anti-cleaved caspase-3	Cell Signaling Technology	Cat#9661; RRID: AB_2341188
Rabbit polyclonal anti-fibrinogen	Gift from J. Degen, Cincinnati	N/A
Mouse monoclonal anti-fibrinogen	Abcam	Cat#ab58207; RRID: AB_941597
Rabbit monoclonal anti-GAPDH	Cell Signaling Technology	Cat#2118; RRID: AB_561053
Rabbit monoclonal anti-GFAP	Cell Signaling Technology	Cat#12389; RRID: AB_2631098
Rat monoclonal anti-GFAP	Thermo Fisher Scientific	Cat#13-0300; RRID: AB_2532994
Rabbit monoclonal anti-phospho-histone H3	Cell Signaling Technology	Cat#3377; RRID: AB_1549592
Rabbit monoclonal anti-Id2	CalBioreagents	Cat#M213; RRID: AB_1151771
Rabbit monoclonal anti-LEF1	Cell Signaling Technology	Cat#2230; RRID: AB_823558
Mouse monoclonal anti-MBP (SMI-94)	BioLegend	Cat#836504; RRID: AB_510039
Rat monoclonal anti-MBP	EMD Millipore	Cat#ab92406; RRID: AB_10562952
Rabbit polyclonal anti-Olig2	EMD Millipore	Cat#ab9610; RRID: AB_570666
Rabbit polyclonal anti-RNF43	Abcam	Cat#ab84125; RRID: AB_2181252
Rabbit monoclonal anti-phospho-Smad1/5	Cell Signaling Technology	Cat#9516; RRID: AB_491015
Rabbit monoclonal anti-phospho-Smad1/5/9	Cell Signaling Technology	Cat#13820; RRID: AB_2493181
Goat polyclonal anti-phospho-Smad1/5/8	Santa Cruz Biotechnology	Cat#sc-12353; RRID: AB_656614
Biological Samples		
Human multiple sclerosis brain sections	Laboratory of D. Reich, NIH	Absinta et al., 2016
Human multiple sclerosis and control brain sections	Laboratory of M. Han, Stanford	Han et al., 2008
Human neonatal hypoxic ischemic encephalopathy brain sections	UCSF Pediatric Neuropathology Research Laboratory	http://ucpnc.pathology.ucsf.edu/; Fancy et al., 2011b
Chemicals, Peptides, and Recombinant Proteins		
Human fibrinogen, plasminogen-depleted	EMD Millipore	Cat#341578-500MG CAS:9001-32-5
Human fibrinogen-Alexa 594 conjugate	Thermo Fisher Scientific	Cat#F13193
Bovine albumin	Sigma-Aldrich	Cat#A4161 CAS:9048-46-8
Bovine albumin-Alexa 594 conjugate	Thermo Fisher Scientific	Cat#A13101
Recombinant human BMP4	Peprotech	Cat#120-05ET
Recombinant human BMP7	Peprotech	Cat#120-03
Recombinant human Noggin	Peprotech	Cat#120-10C
DMH1	Tocris	Cat#4126; CAS:1206711-16-1
Lysolecithin (L-α-Lysophosphatidylcholine) from bovine brain	Sigma-Aldrich	Cat#L1381 CAS:9008-30-4
Ancrod	National Institute for Biological Standards and Control (NIBSC)	Cat#74/581
Tamoxifen	Sigma-Aldrich	Cat#T5648; CAS:10540-29-1
4-hydroxytamoxifen	Tocris	Cat#3412 CAS:68047-06-3
Lipofectamine LTX with PLUS reagent	Thermo Fisher Scientific	Cat#A12621

(*Continued on next page*)

Continued

REAGENT or RESOURCE	SOURCE	IDENTIFIER
Critical Commercial Assays		
EnGen Mutation Detection Kit	New England BioLabs	Cat#E3321S
Rat Gene 1.0 ST GeneChip array	Affymetrix	Cat#901173
Deposited Data		
Raw data files from microarrays	Gene Expression Omnibus	GEO: GSE104450
Experimental Models: Cell Lines		
HAP1 parental control cell line	Horizon	Cat#C631
HAP1 ACVR1 knockout cell line	Horizon	Cat# HZGHC000195c001
Experimental Models: Organisms/Strains		
Rat: Sprague-Dawley	Simonsen Laboratories Charles River	Sim(SD) Crl:SD. Cat#400
Mouse: C57BL/6J	The Jackson Laboratory	JAX: 000664; RRID: IMSR_JAX:000664
Mouse: NG2-CreER™: B6.Cg-Tg(Cspg4-cre/Esr1*) BAkik/J	The Jackson Laboratory; Zhu et al., 2011	JAX: 008538; RRID: IMSR_JAX:008538
Mouse: Rosa-tdTomato: B6.Cg-Gt(ROSA) 26Sor$^{tm14(CAG-tdTomato)Hze}$/J	The Jackson Laboratory; Madisen et al., 2010	JAX: 007914; RRID: IMSR_JAX:007914
Oligonucleotides		
LacZ sgRNA: GTGCGAATACGCCCACGCGAT	Platt et al., 2014	N/A
ACVR1 sgRNA 128, targeting exon 6: GCGCCTGAACCCCAGAGACG	This paper	N/A
For all sgRNA sequences, primers for edited genomic loci, and primers for quantitative PCR, see Table S2.	N/A	N/A
Recombinant DNA		
Plasmid: peSpCas9(1.1)(BB)	Gift from F. Zhang; Slaymaker et al., 2016	Addgene plasmid #71814
Plasmid: peSpCas9(1.1)-fG(BB)	This paper	N/A
Plasmid: pCMV-Cas9-fG(BB)	This paper	N/A
Software and Algorithms		
ImageJ	NIH	https://imagej.nih.gov/ij/; RRID: SCR_003070
Prism 7	GraphPad Software	https://graphpad.com/scientific-software/prism/; RRID: SCR_002798

CONTACT FOR REAGENT AND RESOURCE SHARING

Further information and requests for resources and reagents should be directed to and will be fulfilled by the Lead Contact, Katerina Akassoglou (kakassoglou@gladstone.ucsf.edu).

EXPERIMENTAL MODEL AND SUBJECT DETAILS

Animals

Sprague-Dawley timed-pregnant females or females with litters were purchased from Simonsen Laboratories or Charles River. E15 and P1–P7 rats of both sexes were used for DRG and OPC isolations, respectively. C57BL/6, *NG2-CreER^{TM}* (Zhu et al., 2011), and *Rosa-tdTomato* (Madisen et al., 2010) mice were purchased from the Jackson Laboratory. Heterozygous, male and female *NG2-CreER^{TM}:Rosa-tdTomato* P7 mice were used for *in vitro* OPC fate-mapping studies and 8–12-week-old mice for *in vivo* fate-mapping. All LPC experiments were performed on 8–12-week-old male C57BL/6 mice. Mice were housed in groups of five per cage under standard vivarium conditions and a 12-h light/dark cycle. All animal protocols were approved by the Committee of Animal Research at the University of California, San Francisco, and in accord with the National Institutes of Health guidelines.

Primary OPC Cultures

Rat cortical OPCs were isolated with immunopanning as previously described (Dugas and Emery, 2013) with the following modifications. Cerebral cortices from P1-7 Sprague-Dawley rats were dissected and then digested in papain (Worthington) in DPBS at 35°C

for 30-45 minutes. After trituration, cells were incubated sequentially on three immunopanning dishes: RAN-2 (negative selection), O1 (negative selection), and O4 (positive selection). OPCs were released from the final panning dish with trypsin (Worthington) and seeded onto polyethyleneimine (Sigma-Aldrich)-coated tissue-culture plates or 8-well Permanox-chamber slides (Thermo Scientific Nunc) at an initial density of approximately 15,000 cells per cm^2. OPCs were maintained in a 5% CO_2 incubator at 37°C, first in proliferation media for 2 days, then in differentiation media for up to 4 additional days with a 50% media change after 2 days. The chemically defined base media was DMEM (4.5g/L glucose, +pyruvate, +glutamine; Thermo Fisher Scientific), 1x B27 (Thermo Fisher Scientific), 1x N2 (Thermo Fisher Scientific), 1% penicillin-streptomycin (Thermo Fisher Scientific), and 50 ng ml^{-1} NT3 (Peprotech). Proliferation media consisted of the base media supplemented with 10-20 ng ml^{-1} PDGF-AA (Peprotech). Differentiation media contained 20 ng ml^{-1} CNTF (Peprotech) and 40 ng ml^{-1} triiodothyronine (Sigma-Aldrich) with no PDGF-AA. Experiments were performed after the initial 2 days of proliferation.

OPC-DRG Cultures

OPC-DRG co-cultures were prepared as previously described (Lee et al., 2012). Briefly, DRG neurons from E15 Sprague-Dawley rats were dissociated and plated (150,000 cells per collagen-coated 25-mm coverslip) with 100 ng ml−1 NGF (AbD Serotec). Neurons were maintained in MEM (Thermo Fisher Scientific) supplemented with 10% FBS (Hyclone) and 25 mM glucose. Proliferating cells were selected against with three treatments of 2 mM FDU/Uridine (Sigma-Aldrich). Neurons were maintained for 3 weeks and washed extensively with DMEM (Thermo Fisher Scientific) to remove any residual NGF before seeding OPCs. A2B5+ OPCs were isolated from P7-8 Sprague-Dawley rat brain cortices using immunopanning, and 250,000 cells were plated onto each DRG cover glass. Co-cultures were grown in chemically defined medium composed of DMEM (Thermo Fisher Scientific) supplemented with B27 (Thermo Fisher Scientific), N2 (Thermo Fisher Scientific), penicillin-streptomycin (Thermo Fisher Scientific), N-acetyl-cysteine (Sigma-Aldrich), and forskolin (Sigma-Aldrich).

OPC-Nanofiber Cultures

OPC-nanofiber cultures were prepared as previously described (Lee et al., 2012). Briefly, electron-spun polystyrene fibers (J. M. Corey, Univ. of Michigan) were aligned and secured to 12-mm coverslips with silicone adhesive (Dow Corning), sterilized with 70% ethanol, and coated with 100 μg ml^{-1} poly(L-lysine). Immunopanned O4+ OPCs (200,000 cells per coverslip) were plated onto the coated fibers and maintained in DMEM (Thermo Fisher Scientific) supplemented with B27 (Thermo Fisher Scientific), N2 (Thermo Fisher Scientific), penicillin-streptomycin (Thermo Fisher Scientific), N-acetyl-cysteine (Sigma-Aldrich), and forskolin (Sigma-Aldrich). For the first 2-3 days *in vitro*, the media was supplemented with 12.5 ng ml^{-1} PDGF-AA (Peprotech) to induce proliferation. Thereafter, the media was without PDGF-AA to promote OPC differentiation and myelination.

Macrophage Conditioned Media

Bone marrow-derived macrophages (BMDMs) were isolated from tibia and femur of adult Sprague-Dawley rats as described (Ryu et al., 2015). Bone-marrow cells were cultured in RPMI-1640 medium with 10% heat-inactivated FBS (Invitrogen), 1% penicillin-streptomycin (Corning), and 10 ng/ml rat M-CSF (Peprotech) for 7 d *in vitro* before use. On day 7, adherent BMDMs were dissociated from the plate and re-plated on uncoated or fibrin-coated 24 wells in OPC culture medium. Fibrin coating was prepared as previously described (Ryu et al., 2015). After 24 hours of stimulation, macrophage-conditioned media was collected, clarified by centrifugation, and added to OPC cultures.

HAP1 Cell Cultures

HAP1 cells edited by CRISPR/Cas to contain a 2bp insertion in a coding exon of ACVR1 (HZGHC000195c001) and parental HAP1 control cells (C631) were purchased from Horizon (Cambridge, UK) and cultured in Iscove's Modified Dulbecco's Medium (IMDM) supplemented with 10% FBS and 1% penicillin-streptomycin according to manufacturer's instructions. Cells were serum-starved for 5 hours prior to fibrinogen stimulation.

Human MS and Neonatal HIE Tissue

All human tissue was collected after informed consent and after institutional approval. Brain autopsy samples were collected from patients with different clinical subtypes of MS (Absinta et al., 2016; Fancy et al., 2011b, 2014; Han et al., 2008). Lesions with florid parenchymal and perivascular inflammatory cell infiltration, abundant astroglial hypertrophy, myelin fragmentation, edema and ongoing demyelination with indistinct margins were classified as active lesions (Han et al., 2008). Chronic lesions had areas of demyelination with well-demarcated borders and abundant astrogliosis, but few or no inflammatory cells (Han et al., 2008). Remyelinated lesions were defined as discrete focal areas of pale Luxol fast blue staining but near-normal PLP/myelin immunostaining, with few or no inflammatory cells (Patrikios et al., 2006). Age-matched control brain samples were analyzed similarly and were devoid of CNS abnormalities. Human HIE tissue was collected after informed consent and in accordance with guidelines established by the UCSF Committee on Human Research (H11170-19113-07), as previously described (Fancy et al., 2011b). Tissue was processed and evaluated by UCSF neuropathology staff as described (Fancy et al., 2014).

METHOD DETAILS

Fibrinogen and Pharmacologic Inhibitors

Fibrinogen (EMD Millipore) was used at 2.5 mg ml^{-1}, which is its physiological concentration in plasma (Davalos and Akassoglou, 2012). For signaling experiments, OPCs were factor-starved for 6–15 h before experimental treatments. For analysis of differentiation, OPCs were treated with 2.5 mg ml^{-1} fibrinogen, 50 ng ml^{-1} BMP4 (Peprotech), or 50 ng ml^{-1} BMP7 (Peprotech) when changed to differentiation media. For inhibitor studies, OPCs were pre-treated with 1 μM DMH1 (Tocris), 500–1000 ng ml^{-1} recombinant human noggin (Peprotech), or vehicle (control) 1 h before treatments. In noggin experiments, the inhibitors were also incubated with the vehicle (control)-, fibrinogen-, or BMP-containing differentiation media at 37°C for 1 h before being added to the OPCs. Inhibitors were replaced with subsequent media changes.

Myelinating Cultures

In OPC-DRG cultures, 2.5 mg ml^{-1} fibrinogen was added when OPCs were plated onto DRGs and with media changes every 3 days. In OPC-nanofiber cultures, poly(L-lysine)-coated fibers were additionally coated with fibrinogen (Calbiochem), albumin (A4161, Sigma-Aldrich), fibrinogen-Alexa Fluor 594 or 647 conjugate (Thermo Fisher Scientific), or albumin-Alexa Fluor 594 or 647 conjugate (Thermo Fisher Scientific) at 50 μg ml^{-1} for 2 h at 37° before adding OPCs. Cultures were fixed and processed for immunostaining at 4–6 DIV for OPC-nanofibers and 7–9 DIV for OPC-DRGs.

Cell Fate Mapping Studies

For *in vitro* fate-mapping studies, mouse cortical OPCs were isolated from *NG2-CreER^{TM}:Rosa-tdTomato* mice by immunopanning as previously described (Emery and Dugas, 2013) with the exception that papain digestion occurred in DPBS at 35°C for 30-45 minutes. Cells were incubated sequentially on three immunopanning dishes: BSL1 × 2 (negative selection) and PDGFRα (positive selection). Mouse OPC proliferation and differentiation media has been described previously (Emery and Dugas, 2013). To induce Cre-mediated recombination, OPCs were treated with 1 μM 4-hydroxytamoxifen (Sigma-Aldrich) in proliferation media for 48 hours. Cultures were then changed to control or fibrinogen-containing differentiation media and processed for immunostaining 3 days after the media change. For *in vivo* fate-mapping, 8- to 12-wk-old *NG2-CreER^{TM}:Rosa-tdTomato* mice were injected intraperitoneally with 1 mg tamoxifen (Sigma-Aldrich) daily for four days. Experiments were performed 3-4 weeks after tamoxifen administration.

CRISPR/Cas9-Mediated Knockout of Acvr1 in Primary OPCs

Experimental Overview

One to five days after initial isolation, primary rat OPCs were transfected with a Cas9 expression plasmid expressing EGFP and sgRNA for either LacZ (control) or Acvr1. To determine genome targeting efficiency, transfected OPCs underwent T7 endonuclease I assays three days after transfection. To determine changes in gene expression, cultures 2-4 days after transfection were fibrinogen-treated (2.5 mg ml^{-1} for 2 hours) and then underwent FACS to select the transfected cells for RNA isolation and analysis. In some experiments, OPCs were sorted two days after transfection, re-plated into proliferation media and allowed to recover for two days before fibrinogen treatment and RNA isolation. To assess differentiation, OPCs were transfected at 5 DIV, underwent FACS two days after transfection, re-cultured for two days in proliferation media, and then fibrinogen-treated when changed to differentiation media. Cultures were fixed and processed for immunostaining after 3 days of differentiation.

Plasmids

The plasmid peSpCas9(1.1)(BB) encoding SpCas9 (with improved specificity) was a gift from Dr. Feng Zhang (Addgene plasmid # 71814) (Slaymaker et al., 2016), peSpCas9(1.1)-fG(BB) was constructed by fusing the sequence encoding P2A-farnesylated EGFP to Cas9 in peSpCas9(1.1)(BB). pCMV-Cas9-fG(BB) was constructed by replacing the CBh promoter in peSpCas9(1.1)-fG(BB) with the CMV promoter. The annealed oligonucleotides for the sgRNA guide sequence were ligated to BbsI-digested peSpCas9(1.1)-fG(BB) or pCMV-Cas9-fG(BB). sgRNA guide sequences are listed in Table S2.

OPC Transfection

Primary OPCs cultured in proliferation medium were transfected by adding the plasmid, Lipofectamine LTX and Plus reagent mixed in OPTI-MEM (Thermo Fisher Scientific) according to the manufacturer's instructions. Two μg of plasmids, 2 μL of Plus and 4 μL of Lipofectamine LTX were used to transfect OPCs cultured on a 3.5-cm dish; double the amount was used for cells cultured on 6-cm dishes. After overnight incubation, the medium was replaced.

T7 Endonuclease I Assays

Three days after transfection of cultured OPCs, the cells were lysed in lysis buffer (100 mM NaCl, 10 mM Tris-Cl pH 8.0, 25 mM EDTA, 0.5% SDS, and 0.1 mg/ml proteinase K) at 56°C for 1 hr. Genomic DNA was precipitated by adding double the volume of 100% ethanol and centrifuging at 16100 × *g* for 5 min at room temperature. After washing twice with 70% ethanol and drying, the DNA pellet was dissolved in TE buffer (10 mM Tris-Cl pH 8.0 and 1 mM EDTA) at 56°C for 10 min. The genome editing events were detected

by using the EnGen Mutation Detection Kit (New England BioLabs) and 25-65 ng of genomic DNA according to the manufacturer's instructions. The primer pairs used for PCR amplification of the edited loci are listed in Table S2.

FACS of Transfected OPCs

Two and four days after transfection, cultured OPCs were rinsed twice with Hanks' balanced salt solution without calcium and magnesium (Thermo Fisher Scientific), and then trypsinized with 0.25% trypsin (Thermo Fisher Scientific) in the incubator for 5 min. Cells were resuspended by pipetting and trypsinization was stopped by adding an equal volume of DPBS without calcium and magnesium (Thermo Fisher Scientific) containing 0.25% ovomucoid (Worthington) and 0.25% bovine serum albumin (Sigma-Aldrich). After centrifugation at 300 × *g* for 5 min, the cell pellet was resuspended in 0.4 mL of FACS buffer (DPBS without calcium and magnesium containing 1 × B-27, 1 × N-2, 2 mM EDTA, 5.56 mM glucose, and 25 mM HEPES-Na pH 7.0) and kept on ice. Cell suspension was filtered through a 40 μm cell strainer and EGFP+ cells (MFI cut-off 103) were sorted using the FACSAria II (BD Biosciences). EGFP+ cells were collected into 300 μl FACS buffer at 4°C for RNA isolation, or in 300 μl proliferation medium containing 25 mM HEPES-Na pH 7.0 at room temperature for re-culture experiments. For RNA isolation, sorted cell suspension was centrifuged for 8 minutes at 300 X g at 4°C and the cell pellet lysed in 350 μl RLT buffer with 1% 2-mercaptoethanol (Sigma). For re-culture experiments, sorted cells were re-plated into proliferation media and allowed to recover for two days before fibrinogen treatment.

RNA Isolation and Quantitative PCR

Total RNA was extracted from OPC cultures with the RNeasy kit (QIAGEN) according to the manufacturer's instructions. cDNA was generated and real-time (RT)-PCR performed as previously described (Ryu et al., 2015). Data are expressed as $2^{-\Delta\Delta C}{}_T$ for the experimental gene-of-interest normalized against the housekeeping gene and presented as the fold change versus the relevant control. Primers are listed in Table S2.

Gene-Expression Profiling by Microarray Analysis

Microarray analysis was performed on triplicate samples of primary rat OPCs treated with 2.5 mg ml^{-1} fibrinogen for 12 h and 48 h in differentiation media. Total RNA was isolated using RNeasy Mini kit (QIAGEN) according to the manufacturer's instruction. Probes were prepared using NuGEN Ovation Pico WTA V2 kit and NuGEN Encore Biotin Module, and hybridized to Rat Gene 1.0 ST GeneChip arrays (Affymetrix). Arrays were scanned using an Affymetrix GCS3000 scanner and Affymetrix Command Console software, and data were normalized using the RMA algorithm in Affymetrix Expression Console. Microarrays were normalized for array-specific effects using Affymetrix's 'Robust Multi-Array' normalization. Normalized array values were reported on a log2 scale. For statistical analyses, we removed all array probe sets where no experimental groups had an average log2 intensity > 3.0. This is a standard cutoff, below which expression is indistinguishable from background noise. Linear models, moderated *t*-statistics, fold change, false discovery rate (FDR)-adjusted values, and the associated *P* values were calculated as described (Ryu et al., 2015).

Immunoblots

Cells were lysed in cell lysis buffer supplemented with protease/phosphatase inhibitor cocktails (Calbiochem) and lysates were cleared by centrifuging at 13,000x*g* for 15 minutes at 4°C. Equal amounts of protein were loaded in 4%–12% or 8%–16% gels and analyzed by western blotting. Bands were visualized with HRP-conjugated secondary antibodies (Cell Signaling Technology or Santa Cruz Biotechnology). Densitometry was performed using ImageJ Software (NIH) with values for each band normalized to GAPDH loading controls from the same membrane.

Immunocytochemistry, Immunohistochemistry, and *In Situ* Hybridization

Immunocytochemistry (ICC) was performed as previously described (Lee et al., 2012). Briefly, cultures were fixed with 4% PFA for 15 min at room temperature, permeabilized, and blocked by incubation with 10%–20% goat or donkey serum (Sigma-Aldrich or Jackson ImmunoResearch) and 0.1%–0.2% Triton X-100 (Sigma-Aldrich) in PBS. Primary antibody incubations were performed overnight at 4°C. Fluorescent secondary antibodies (Jackson ImmunoResearch or Thermo Fisher Scientific) were incubated for 1–2 h at room temperature. DAPI was used to detect cell nuclei.

For mouse immunohistochemistry (IHC), mice were transcardially perfused with 4% PFA under deep avertin anesthesia. Tissue was removed, post-fixed overnight in 4% PFA, cryoprotected in 30% sucrose/PBS, frozen in Neg-50 media (Thermo Scientific), cryosectioned into 12-μm sections, and placed on ColorFrost Plus microscope slides (Fisher Scientific). Sections were permeabilized in 0.1% Triton X-100, blocked with 5% BSA or 5% normal donkey serum, and incubated with primary antibodies overnight at 4°C and then fluorescent secondary antibodies for 1–2 h at room temperature. Slides were coverslipped with Prolong Gold or SlowFade Gold antifading agent with DAPI (Thermo Fisher Scientific). *In situ* labeling of the mature oligodendrocyte marker *PLP* was performed as previously described (Fancy et al., 2011b).

For human IHC, formalin-fixed paraffin embedded tissue sections were first deparaffinized then rehydrated. Heat-mediated antigen retrieval was performed with Target Retrieval Solution, Low pH (Dako) for 1 hour in 95° water bath. Endogenous alkaline phosphatase and horseradish peroxidase activity was blocked with Bloxall (Vector). Sections were permeabilized in 0.3% Triton X-100, blocked with 2.5% normal horse serum, and incubated with primary antibodies overnight at 4°C. Sequential labeling of multiple

antigens was performed using the ImmPRESS-AP Anti-Mouse IgG (alkaline phosphatase) and ImmPRESS VR Anti-Rabbit IgG HRP Kits (Vector) and developed with the Vector Blue or NovaRED Substrate Kits (Vector) according to manufacturer's instruction. Slides were coverslipped in VectaMount AQ (Vector).

Images were acquired with an Axioplan II epifluorescence microscope (Carl Zeiss) equipped with dry Plan-Neofluar objectives (10x 0.3 NA, 20x 0.5 NA, or 40x 0.75 NA), an Axiocam HRc CCD camera, and the Axiovision image analysis software; the BIOREVO BZ-9000 inverted fluorescence microscope (Keyence) equipped with a Nikon CFI 60 Series infinite optical system and Keyence imaging software; or Olympus Fluoview confocal microscope equipped with 20x NA1.0 objective. All images were processed and analyzed in ImageJ. For ICC, cell counts from multiple wells (5–10 images per well) from two or more independent experiments were quantified for each test group. For IHC in the brain, cell counts from multiple 200μm x 200μm randomly selected regions of interest within 250μm of the cannula tract were quantified on two or more nonadjacent sections per mouse. N = 6-8 mice per group. In the spinal cord, quantification was performed on thresholded images. N = 3-4 mice per group. For ISH, PLP-positive cells were counted within lesions on three or more nonadjacent sections per mouse with N = 3-4 mice per group.

The following primary antibodies were used: cleaved caspase-3 (ICC: 1:200, rabbit polyclonal, #9661, Cell Signaling Technology); fibrinogen (mouse IHC: 1:1000, rabbit polyclonal, gift from J. Degen, Cincinnati; human IHC: 1:500, mouse monoclonal, #ab58207, Abcam); GAPDH (WB: 1:1000, rabbit monoclonal, #2118, Cell Signaling Technology); GFAP (ICC/IHC: 1:200, WB: 1:1000, rabbit monoclonal, #12389, Cell Signaling Technology; or rat monoclonal, #13-0300, Thermo Fisher Scientific); phospho-histone H3 (ICC: 1:200, rabbit monoclonal, #3377, Cell Signaling Technology); Id2 (human IHC: 1:1000, rabbit monoclonal, # M213, CalBioreagents); LEF1 (ICC: 1:200, WB: 1:1000, rabbit monoclonal, #2230, Cell Signaling Technology); MBP (ICC/IHC: 1:500, WB: 1:1000, mouse monoclonal, SMI-94, BioLegend; or rat monoclonal, #ab92406, EMD Millipore); Olig2 (ICC/IHC: 1:200, rabbit polyclonal, #ab9610, EMD Millipore); RNF43 (IHC: 1:200, rabbit polyclonal, #ab84125, Abcam); phospho-Smad1/5 (WB: 1:1000, rabbit monoclonal, #9516, Cell Signaling Technology); phospho-Smad1/5/9 (WB: 1:1000, ICC: 1:200, rabbit monoclonal, #13820, Cell Signaling Technology); and phospho-Smad1/5/8 (IHC: 1:100, goat polyclonal, #sc-12353, Santa Cruz Biotechnology).

Chronic Fibrinogen Infusion

Fibrinogen was infused continuously into the brains of tamoxifen-induced *NG2-CreER^{TM}:Rosa-tdTomato* mice using mini-osmotic pumps (ALZET model 2002, 0.5 μl/h for 14 d) and the brain infusion kit (ALZET Brain infusion kit 3) according to the manufacturer's instruction. Pumps were filled with either fibrinogen (2 mg ml^{-1}) or artificial CSF and primed for 24 h at 37°C. The sterile brain infusion cannula (30-gauge) was stereotactically implanted at the following coordinates: 0.5 mm rostral to the bregma, 1 mm lateral to the midline, and 2 mm deep from the skull surface. The cannula was glued to the skull using Metabond (Parkell) and dental cement, while the pump was inserted subcutaneously on the back. Mice were euthanized for histological analysis after 14 day infusion.

Lysolecithin-Induced Focal Demyelination

Demyelinated lesions were chemically induced by focal injection of lysolecithin into the spinal cord ventrolateral white matter of 8- to 12-wk-old C57BL/6 mice as previously described (Mei et al., 2014) with modifications highlighted in the following experimental description. Animals were anesthetized via intraperitoneal injection of ketamine (100 mg/kg) and xylazine (15 mg/kg). A midline skin incision was made over the upper lumbar regions of spinal cord, and the spinal column was secured with mouse vertebral clamps fixed in a stereotaxic frame. The epidural space was exposed by disruption of the L1-L2 interspinous ligament without laminectomy as described (Ryu et al., 2015). A pulled-glass micropipette secured to a Hamilton syringe was prefilled with 1% lysolecithin (L-α-lysophosphatidylcholine, Sigma-Aldrich) and inserted into the spinal cord 0.3 mm lateral to the spinal midline and a depth of 0.9 mm from the spinal cord surface. Then, 1 μL of 1% lysolecithin was injected (0.2 μl/min) and the glass micropipette remained in place for 5 min before being slowly withdrawn. After surgery, skin was sutured, and mice were allowed to recover.

Pharmacologic Depletion of Fibrinogen after Lysolecithin Injection

Mice were depleted of fibrinogen with ancrod at 3 d.p.l. as described (Adams et al., 2007). The mice received 2.75 U ancrod/day by mini-osmotic pump (Alzet). In control animals, buffer-filled mini-pumps were implanted.

Electron Microscope Analysis of Remyelination

At 14 days post-lysolecithin injection, mice were transcardially perfused with 2% PFA/2.5% glutaraldehyde in 0.1 M sodium cacodylate buffer with 2 mM $CaCl_2$. Spinal cords were processed and EM performed with a FEI Spirit transmission electron microscope, according to standard procedures (Davalos et al., 2012). We examined ~300 axons (~75 axons per mouse, N = 4 mice per group) within the rim of active remyelination at the lesion edge, and calculated g-ratios as the diameter of the axon divided by the diameter of the axon plus the surrounding myelin sheath. Unmyelinated axons were excluded from G-ratio graph and analysis.

QUANTIFICATION AND STATISTICAL ANALYSIS

Data are presented as mean ± standard error of the mean. Differences between experimental conditions were analyzed with GraphPad Prism software. Data distribution was assumed to be normal, but this was not formally tested. No statistical methods were used to predetermine sample size, but our sample sizes are similar to those reported (Fancy et al., 2014). Mice and cells were divided into experimental groups in an unbiased manner. No randomization was used to assign groups or to collect data. All animals survived until the end of the study, and all data points were included in analysis. Analyses of *in vitro* inhibitor, CRISPR, and conditioned media experiments were performed by a blinded observer. The unpaired Student's t test was used for isolated pairs, and two-way analysis of variance (ANOVA) with a Bonferroni or Holm-Sidak post-test was used for multiple comparisons. $p < 0.05$ was considered significant.

DATA AND SOFTWARE AVAILABILITY

The raw data files from the microarrays have been deposited in the Gene Expression Omnibus under GEO: GSE104450.

Neuron, Volume *96*

Supplemental Information

Fibrinogen Activates BMP Signaling in Oligodendrocyte Progenitor Cells and Inhibits Remyelination after Vascular Damage

Mark A. Petersen, Jae Kyu Ryu, Kae-Jiun Chang, Ainhoa Etxeberria, Sophia Bardehle, Andrew S. Mendiola, Wanjiru Kamau-Devers, Stephen P.J. Fancy, Andrea Thor, Eric A. Bushong, Bernat Baeza-Raja, Catriona A. Syme, Michael D. Wu, Pamela E. Rios Coronado, Anke Meyer-Franke, Stephanie Yahn, Lauriane Pous, Jae K. Lee, Christian Schachtrup, Hans Lassmann, Eric J. Huang, May H. Han, Martina Absinta, Daniel S. Reich, Mark H. Ellisman, David H. Rowitch, Jonah R. Chan, and Katerina Akassoglou

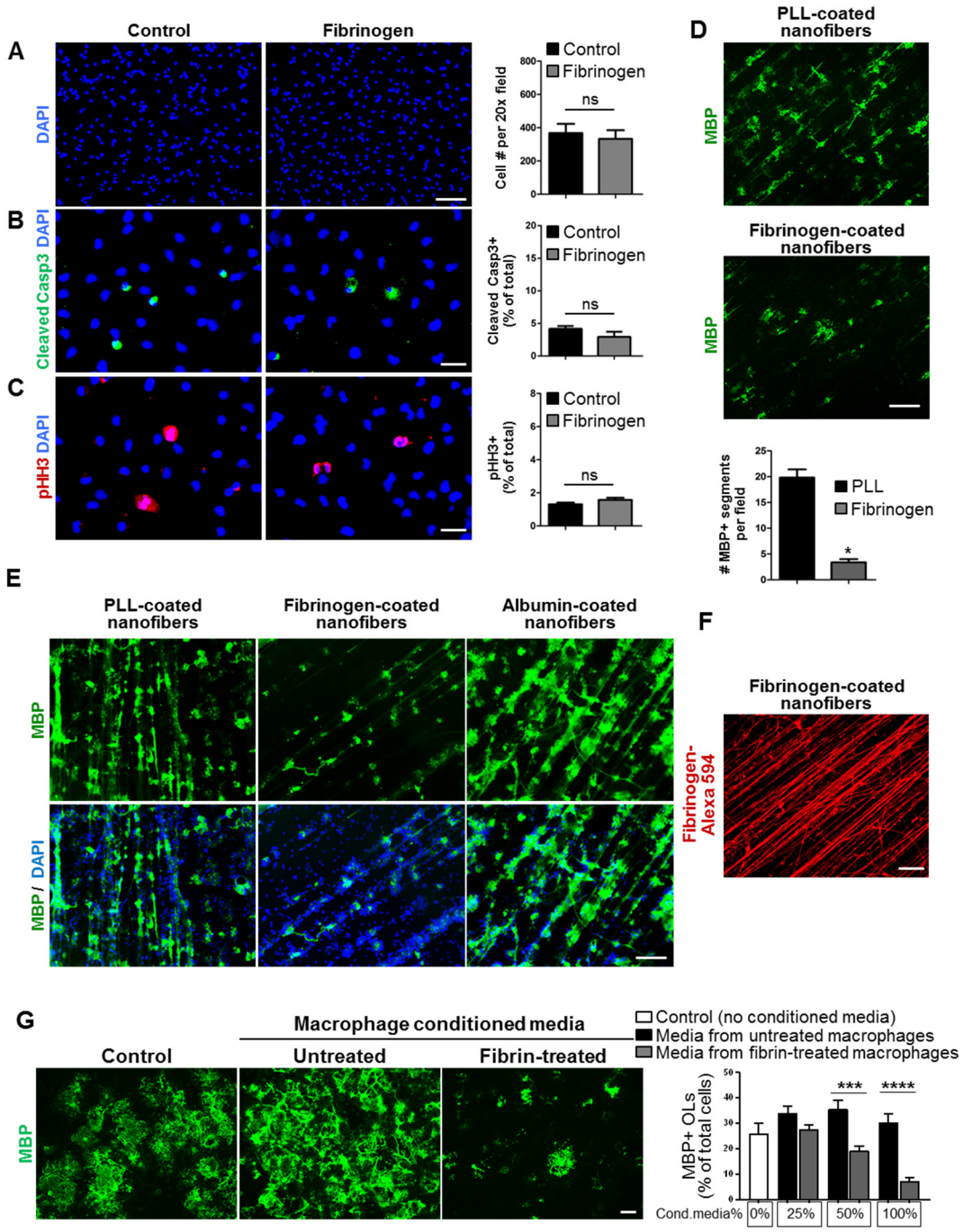

Figure S1. Related to Figure 1. Untreated control and fibrinogen-treated primary rat OPCs analyzed for: (**A**) Cell density. Number of cell nuclei per 20x field after 3 days of treatment. Scale bar: 100 µm. (**B**) Apoptosis**.** Percentage of cells positive for the apoptosis marker cleaved caspase-3 (green) after 1 day of treatment. Scale bar: 25 µm. (**C**) Proliferation**.** Percentage of cells positive for the mitosis marker phospho-histone H3 (red) after 1 day of treatment. Scale bar: 25 µm. All images are representative of n = 3 independent experiments. Nuclei are stained with DAPI (blue).Values are mean ± s.e.m. ns = not significant (unpaired t-test). (**D,E**) MBP+ mature OLs (green) in myelinating cultures of OPCs on control poly-l-lysine (PLL)-coated, fibrinogen-coated, or albumin-coated nanofibers at 4-6 days *in vitro*. Scale bar: 100 µm. Images and quantification are representative of n = 2 independent experiments. Values are mean ± s.e.m. *p<0.05 (unpaired t-test). (**F**) Fibrinogen-coated nanofibers (red, Fibrinogen-Alexa 594). Scale bar: 100 µm. (**G**) MBP immunostaining (green) indicating mature OLs in primary rat OPCs exposed to conditioned media from untreated or fibrin-treated macrophages or no conditioned media (control) for 3 days. Representative images and quantification from n = 3 independent experiments. The percentage of the media volume that was conditioned media is indicated. Scale bar: 50 µm. Values are mean ± s.e.m., ***p < 0.001, ****p<0.0001 (two-way ANOVA with Bonferroni).

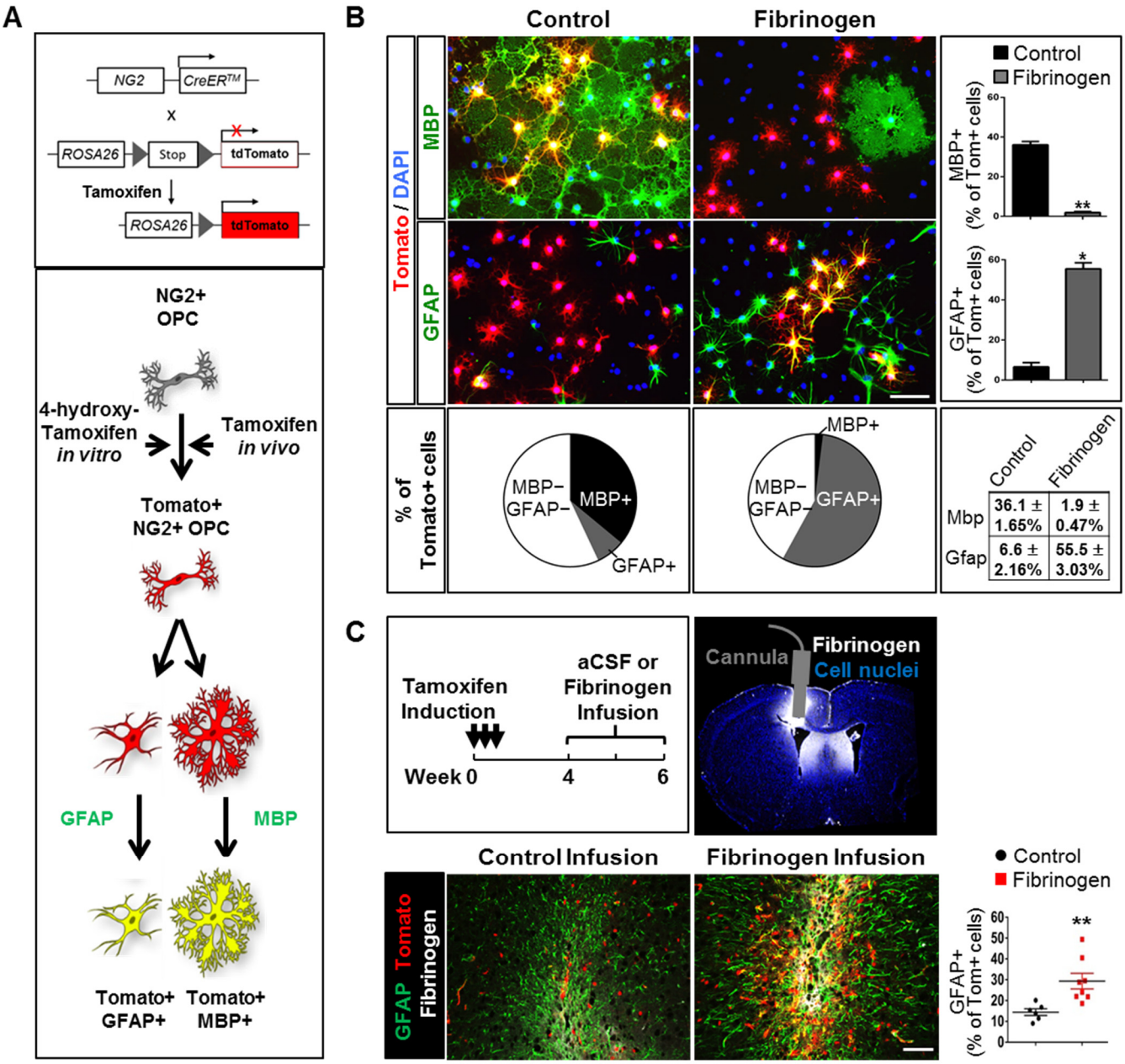

Figure S2. Related to Figure 2H. (**A**) Schematic representation of cell-fate mapping of myelinating MBP+ OLs and astrocyte-like GFAP+ cells derived from *NG2-CreER^{TM}:Rosa-tdTomato* mouse OPCs. **(B)** Cell-fate mapping of fibrinogen-treated *NG2-CreER^{TM}:Rosa-tdTomato* primary mouse OPCs (red) stained for either MBP (green) or GFAP (green). Nuclei are stained with DAPI (blue). Quantification of tdTomato+ OPCs that differentiate into MBP+ OLs or GFAP+ astrocyte-like cells (yellow cells). Values are mean ± s.e.m. from n = 2 independent experiments. *p < 0.05, **p < 0.01 (unpaired *t*-test). Scale bar: 50 µm. (**C**) **Top:** Experimental design for chronic fibrinogen infusion into the *NG2-CreER^{TM}:Rosa-tdTomato* mouse brain in vivo. Representative image of cannula location and deposition of fibrinogen (white) after chronic fibrinogen infusion. Nuclei are stained with DAPI (blue). **Bottom:** Representative images of tdTomato+ OPC-derived cells (red), GFAP (green), and fibrinogen deposition (white) in the brains of *NG2-CreER^{TM}:Rosa-tdTomato* mice after chronic aCSF (control) or fibrinogen infusion. Quantification of percentage of tdTomato+ cells that are also GFAP+ (yellow cells). Values are mean ± s.e.m. from n = 6 (aCSF control) or 8 (fibrinogen infusion) mice. **p < 0.01 (unpaired *t*-test). aCSF: artificial cerebrospinal fluid

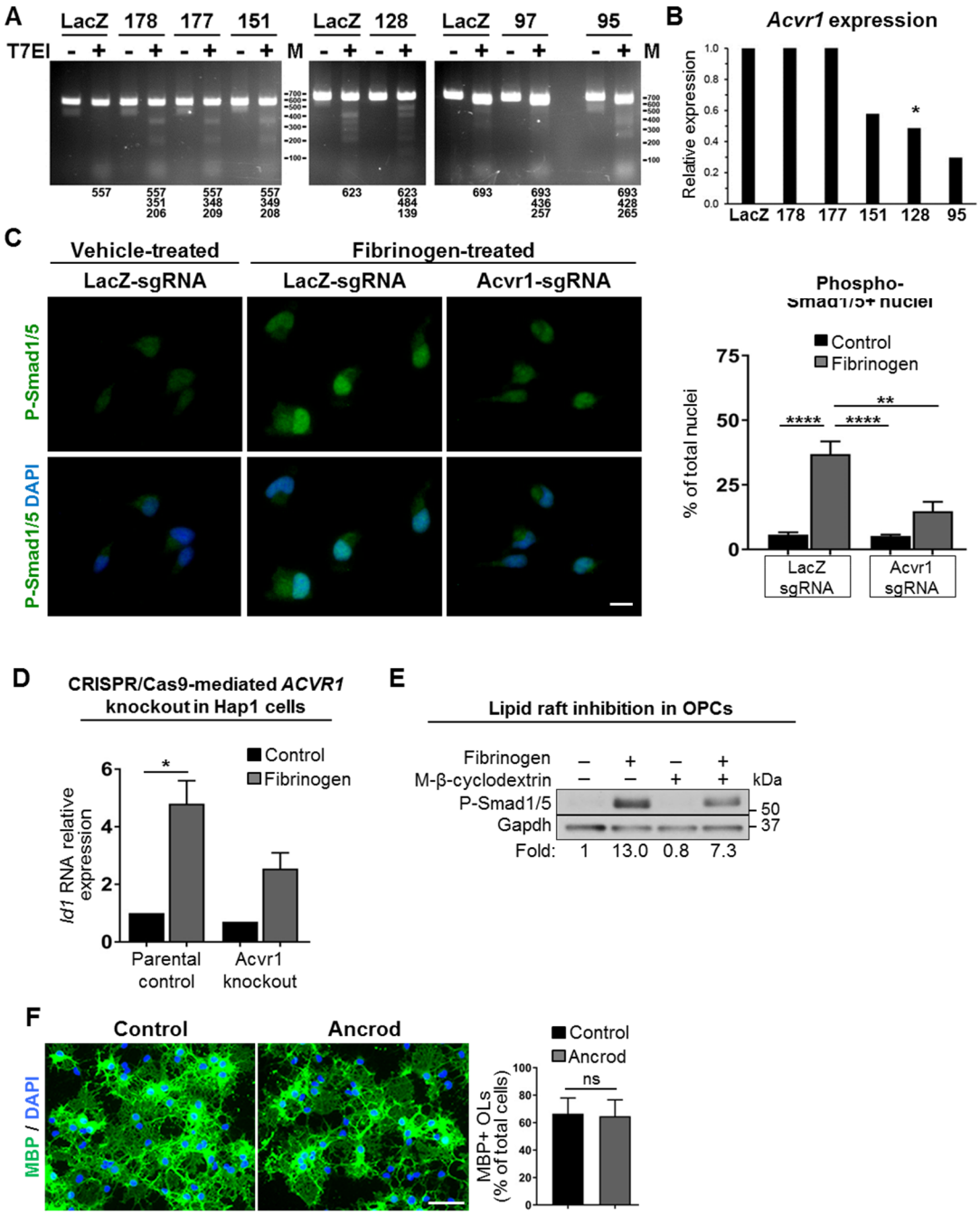

Figure S3. Related to Figure 3C and 4. (**A-B**) Validation of single guide RNA (sgRNA) knockout efficiency. (**A**) T7 endonuclease I assays of Acvr1 sgRNAs 178, 177, 151, 128 and 95. The predicted length (bp) of the PCR and cleavage products is listed below the gel images. M, molecular markers in bp. (**B**) *Acvr1* gene expression in sorted GFP+ OPCs two days after transfection. * Acvr1 sgRNA 128 was used for subsequent experiments. (**C**) Phospho-Smad1/5 immunostaining (green) in primary rat OPCs transfected with sgRNA for LacZ or Acvr1 and vehicle- or fibrinogen-treated for 1 hour. Nuclei are stained with DAPI (blue). Representative images and quantification from n = 4 wells from 2 independent experiments. Scale bar: 25 μm. Values are mean ± s.e.m., **p < 0.01, ****p < 0.0001 (two-way ANOVA with Bonferroni). (**D**) *Id1* gene expression in parental control or Acvr1 knockout Hap1 cells after 3h fibrinogen treatment, n = 2 independent experiments. *p < 0.05 (two-way ANOVA with Bonferroni). (**E**) P-Smad1/5 levels in untreated control or fibrinogen-treated primary rat OPCs in the presence of the lipid raft inhibitor methyl-β-cyclodextrin. Representative immunoblot and mean values from n = 3 independent experiments. (**F**) MBP immunostaining (green) indicating mature OLs in untreated control or ancrod-treated (0.04 IU/ml) primary rat OPC cultures after 3 days. Nuclei are stained with DAPI (blue). Representative images and quantification from n = 2 independent experiments. Scale bar: 50 μm. Values are mean ± s.e.m., ns = not significant (unpaired *t*-test).

Table S1. Related to Figure 1F. Genome-wide analysis of fibrinogen-treated primary rat OPCs analyzed for Gene Ontology (GO) Biological Process (all listed pathways with FDR and adjusted P-value ≤ 0.05)

GO Term: Biological Process	Z score	# of differentially-expressed genes in this gene set	# of genes in this gene set that were on the chip	% changed
cholesterol biosynthetic process (GO:0006695)	11.76	12	22	54.55
developmental process (GO:0032502)	11.06	242	3076	7.87
regulation of cellular component organization (GO:0051128)	9.95	102	978	10.43
positive regulation of cellular process (GO:0048522)	9.89	194	2437	7.96
cellular component organization (GO:0016043)	9.43	190	2442	7.78
negative regulation of cellular process (GO:0048523)	8.69	164	2105	7.79
regulation of microtubule-based process (GO:0032886)	8.53	20	90	22.22
regulation of developmental process (GO:0050793)	8.19	104	1174	8.86
negative regulation of protein kinase activity (GO:0006469)	8.13	23	121	19.01
triglyceride metabolic process (GO:0006641)	8.13	12	40	30.00
response to organic substance (GO:0010033)	7.85	121	1488	8.13
response to external stimulus (GO:0009605)	7.54	77	821	9.38
regulation of cell cycle (GO:0051726)	7.42	54	501	10.78
response to endogenous stimulus (GO:0009719)	7.24	78	862	9.05
multicellular organismal process (GO:0032501)	7.23	142	1936	7.33
cell cycle process (GO:0022402)	7.13	47	424	11.08
cell adhesion (GO:0007155)	7.13	53	505	10.50
response to abiotic stimulus (GO:0009628)	6.99	59	599	9.85
regulation of BMP signaling pathway (GO:0030510)	6.98	12	50	24.00
negative regulation of response to stimulus (GO:0048585)	6.83	52	510	10.20
cellular response to chemical stimulus (GO:0070887)	6.65	78	916	8.52
regulation of programmed cell death (GO:0043067)	6.57	82	989	8.29
cell cycle (GO:0007049)	6.49	31	250	12.40
positive regulation of metabolic process (GO:0009893)	6.35	107	1438	7.44
positive regulation of catalytic activity (GO:0043085)	6.35	60	661	9.08
negative regulation of signalling (GO:0023057)	6.19	44	436	10.09
Locomotion (GO:0040011)	6.16	53	569	9.31
regulation of epithelial cell proliferation (GO:0050678)	6.16	24	179	13.41
regulation of platelet activation (GO:0010543)	6.16	6	18	33.33
regulation of cellular component movement (GO:0051270)	6.05	38	360	10.56
regulation of lipid metabolic process (GO:0019216)	6.04	23	171	13.45
Growth (GO:0040007)	5.99	32	283	11.31
response to stress (GO:0006950)	5.96	116	1652	7.02
regulation of cellular catabolic process (GO:0031329)	5.90	38	368	10.33
enzyme linked receptor protein signaling pathway (GO:0007167)	5.89	34	314	10.83
response to oxygen levels (GO:0070482)	5.85	31	276	11.23
regulation of cell-cell adhesion (GO:0022407)	5.76	11	56	19.64
regulation of fibroblast growth factor receptor signaling pathway (GO:0040036)	5.75	6	20	30.00
regulation of canonical Wnt receptor signaling pathway (GO:0060828)	5.64	16	105	15.24
cell division (GO:0051301)	5.61	21	161	13.04
regulation of hydrolase activity (GO:0051336)	5.45	51	590	8.64
chromosome segregation (GO:0007059)	5.40	10	52	19.23
regulation of ERK1 and ERK2 cascade (GO:0070372)	5.39	15	100	15.00
regulation of growth (GO:0040008)	5.37	39	412	9.47
cell-cell signaling involved in cell fate commitment (GO:0045168)	5.35	7	29	24.14
regulation of mesenchymal cell proliferation (GO:0010464)	5.28	8	37	21.62

response to drug (GO:0042493)	5.26	40	434	9.22
synaptic vesicle transport (GO:0048489)	5.18	8	38	21.05
regulation of chromosome segregation (GO:0051983)	4.98	5	18	27.78
glycoprotein metabolic process (GO:0009100)	4.95	10	58	17.24
response to acid (GO:0001101)	4.94	15	110	13.64
sphingolipid metabolic process (GO:0006665)	4.80	11	70	15.71
regulation of Notch signaling pathway (GO:0008593)	4.79	6	26	23.08
organic acid biosynthetic process (GO:0016053)	4.64	21	193	10.88
regulation of immune system process (GO:0002682)	4.62	45	557	8.08
intracellular signal transduction (GO:0035556)	4.54	69	979	7.05
neutral amino acid transport (GO:0015804)	4.54	6	28	21.43
amino acid transmembrane transport (GO:0003333)	4.54	8	45	17.78
regulation of cellular localization (GO:0060341)	4.47	40	486	8.23
neurotransmitter transport (GO:0006836)	4.46	12	87	13.79
membrane lipid biosynthetic process (GO:0046467)	4.42	6	29	20.69
Phosphorylation (GO:0016310)	4.36	58	802	7.23
response to cadmium ion (GO:0046686)	4.19	7	40	17.50
DNA replication (GO:0006260)	4.18	12	93	12.90
lipid homeostasis (GO:0055088)	4.17	9	60	15.00
fatty acid metabolic process (GO:0006631)	4.15	21	212	9.91
regulation of smooth muscle cell proliferation (GO:0048660)	4.11	11	83	13.25
phospholipid biosynthetic process (GO:0008654)	4.06	12	96	12.50
peptidyl-tyrosine dephosphorylation (GO:0035335)	4.02	7	42	16.67
Notch signaling pathway (GO:0007219)	4.02	8	52	15.38
regulation of transport (GO:0051049)	3.99	55	785	7.01
regulation of protein localization (GO:0032880)	3.90	24	268	8.96
coenzyme metabolic process (GO:0006732)	3.86	17	167	10.18
apoptosis (GO:0006915)	3.84	30	366	8.20
ensheathment of neurons (GO:0007272)	3.82	8	55	14.55
epithelial cell proliferation (GO:0050673)	3.79	7	45	15.56
amine biosynthetic process (GO:0009309)	3.62	13	120	10.83
carbohydrate utilization (GO:0009758)	3.60	137	2460	5.57
regulation of homeostatic process (GO:0032844)	3.60	19	206	9.22
regulation of binding (GO:0051098)	3.57	15	149	10.07
regulation of peptidyl-tyrosine phosphorylation (GO:0050730)	3.56	13	122	10.66
regulation of reproductive process (GO:2000241)	3.35	10	88	11.36
Wnt receptor signaling pathway (GO:0016055)	2.89	13	144	9.03

Table S2. Oligonucleotides

Oligonucleotide pairs for sgRNAs for CRISPR/Cas9-mediated knockout (guide sequences underlined)		
LacZ (Platt et al., 2014)	CACCGTGCGAATACGCCCACGCGAT	AAACATCGCGTGGGCGTATTCGCAC
Acvr1 178 (exon 5)	CACCGCCATCATTGACGCTCAGGG	AAACCCCTGAGCGTCAATGATGGC
Acvr1 177 (exon 5)	CACCGAAGCCATCATTGACGCTCA	AAACTGAGCGTCAATGATGGCTTC
Acvr1 151 (exon 5)	CACCGCAACAGGAACGTCACGGCC	AAACGGCCGTGACGTTCCTGTTGC
Acvr1 128 (exon 6)	CACCGCGCCTGAACCCCAGAGACG	AAACCGTCTCTGGGGTTCAGGCGC
Acvr1 97 (exon 8)	CACCACCTCCCGTGATGAGAAGTCG	AAACCGACTTCTCATCACGGGAGGT
Acvr1 95 (exon 8)	CACCGAACCACGACTTCTCATCAC	AAACGTGATGAGAAGTCGTGGTTC
Primer pairs for PCR amplification of CRISPR/Cas9 edited genomic loci		
Acvr1, intron 4 to intron 5	GGTTTGGGGTGATCTTAG	CCTTCTCCTTTTAGATTCCAAAG
Acvr1, intron 5 to intron 6	TATCATAGCGTCCGTCAG	CTTTGCACACTGGAAATAAGG
Acvr1, intron 7 to intron 8	CCAGAACCCAAATCTAGC	CATAACCTATGTGCGGAC
Primer pairs for quantitative PCR		
Acvr1	ACTGTACGCTGTCAGGCTCTC	CTTGGGCTCCTCATCTTCCATA
β-actin	GAAGAGCTATGAGCTGCCTGAC	AGGTCTTTACGGATGTCAACGT
Id1	TGGACGAACAGCAGGTGAAC	TCTCCACCTTGCTCACTTTGC
Id2	CTCCAAGCTCAAGGAACTGG	GTGCTGCAGGATTTCCATCT
Id3	TGCTACGAGGCGGTGTGCTG	AGTGAGCTCAGCTGTCTGGATCGG
Lef1	GCAGCTATCAACCAGATCC	GATGTAGGCAGCTGTCATTC
Mbp	ATGGCATCACAGAAGAGACCCTCA	TAAAGAAGCGCCCGATGGAGTCAA